

Pharmacological inhibition of FSGS-related TRPC6 gain of function mutants by semisynthetic larixol-derived compounds

Nicole Urban^{*1}, Sonja Neuser^{*1}, Anika Hentschel², Sebastian Köhling², Jörg Rademann²,
Michael Schaefer¹

¹: Rudolf-Boehm-Institut für Pharmakologie und Toxikologie, Universität Leipzig, Leipzig, Germany

²: Institut für Pharmazie, Freie Universität Berlin, Berlin, Germany

*: equal contribution

Running title: Inhibitors of FSGS-related TRPC6 channel mutants

Corresponding author: Michael Schaefer, Rudolf-Boehm-Institut für Pharmakologie und Toxikologie, Härtelstr. 16-18, 04107 Leipzig, Germany, phone: +49 341 9724600, fax: +49 341 9724609, e-mail: michael.schaefer@medizin.uni-leipzig.de

Word count:

- Abstract: 247

- Text body without methods, figure legends and references: 5307

- Discussion: 1946

- References: 50

- Figures: 11

- Tables: 2

Supporting materials: 3 figures, 1 table

Abbreviations:

[Ca²⁺]_i, intracellular Ca²⁺ concentration; FSGS, focal segmental glomerulosclerosis; TRPC, transient receptor potential canonical; HBS, HEPES-buffered solution; HEK, human embryonic kidney; HEK_{hTRPC6-YFP}, HEK293 cells stably expressing human TRPC6 C-terminally fused to yellow fluorescent protein

This article has been accepted for publication and undergone full peer review but has not been through the copyediting, typesetting, pagination and proofreading process which may lead to differences between this version and the Version of Record. Please cite this article as doi: 10.1111/bph.13977

Abstract

Background and purpose

Gain of function mutations in TRPC6 can cause autosomal dominant forms of focal segmental glomerulosclerosis (FSGS). Validated inhibitors of TRPC6 that are biologically active on FSGS-related TRPC6 mutants are eagerly sought.

Experimental approach

We synthesized new TRPC6-inhibiting modulators from larixol, a resiniferous constituent of *Larix decidua*, and tested the potency and selectivity in cell lines stably expressing various TRP channel isoforms. Channel activation was followed by Ca^{2+} influx analyses and electrophysiological recordings. The most promising compound larixyl carbamate (LC) was tested on native TRPC6 and TRPC6 constructs carrying FSGS-related point mutations.

Key results

LC exhibited an about 30-fold and 5-fold preference for TRPC6 versus TRPC3 and TRPC6 versus TRPC7, respectively. Six FSGS-related TRPC6 mutants, including the highly active M132T and R175Q variants, were strongly inhibited by 1 μM larixyl carbamate. We next sought to identify TRPC6-like Ca^{2+} signals in primary murine podocytes, or in acutely isolated glomeruli. Surprisingly, no TRPC6-related Ca^{2+} signals were detectable in these preparations. Quantitative PCR revealed a 20- to 50-fold lower abundance of TRPC6 transcripts in rat or mouse podocytes compared to pulmonary artery smooth muscle cells from the same species. Accordingly, electrophysiological recordings demonstrated that diacylglycerol-induced currents in murine podocytes are very small, but sensitive to LC.

Conclusion and implications

We conclude that, despite low abundance in native podocytes, the native TRPC6 channel is targetable using larixol-derived TRPC6 inhibitors. Like wild-type TRPC6, FSGS-related TRPC6 mutants are sensitive to the newly developed inhibitors, thus, paving the way for experimental therapies.

List of hyperlinks used in MS# 2016-BJP-0904-RP.R2

Targets:

TRPC3: <http://www.guidetopharmacology.org/GRAC/ObjectDisplayForward?objectId=488>

TRPC6: <http://www.guidetopharmacology.org/GRAC/ObjectDisplayForward?objectId=491>

TRPC7: <http://www.guidetopharmacology.org/GRAC/ObjectDisplayForward?objectId=492>

Ligands:

angiotensin II: <http://www.guidetopharmacology.org/GRAC/LigandDisplayForward?ligandId=2504>

bradykinin: <http://www.guidetopharmacology.org/GRAC/LigandDisplayForward?ligandId=649>

carbachol: <http://www.guidetopharmacology.org/GRAC/LigandDisplayForward?ligandId=298>

flufenamic acid: <http://www.guidetopharmacology.org/GRAC/LigandDisplayForward?ligandId=4191>

SKF-96365: <http://www.guidetopharmacology.org/GRAC/LigandDisplayForward?ligandId=2441>

thapsigargin: <http://www.guidetopharmacology.org/GRAC/LigandDisplayForward?ligandId=5351>

Introduction

Focal segmental glomerulosclerosis (FSGS) is one of the leading causes of steroid-resistant nephrotic syndrome and terminal kidney failure in children and adolescents. FSGS is a histopathological finding which in most cases correlates with podocyte injury. In FSGS, the slit diaphragm formed by intercalating foot processes of podocytes is severely disturbed. As a consequence, the filtration barrier cannot retain proteins, and a progressive proteinuria develops, finally culminating in end-stage renal disease and nephrotic syndrome. Inheritable forms of FSGS can be caused by missense or nonsense mutations in proteins that are enriched in podocyte foot processes (e.g. nephrin, podocin, or CD2-associated protein) or in proteins that impact on podocyte function in more complex and indirect ways (Sprangers *et al.*, 2016). Of them, the identification of missense mutations in the TRPC6 gene in autosomal dominant FSGS establishes TRPC6 as a potential pharmacological target (Winn *et al.*, 2005; El & Reiser, 2011). Both gain of function and loss of function mutations in TRPC6 have been identified in autosomal dominant forms of FSGS (Riehle *et al.*, 2016). Of note, the onset of disease seems to correlate with functional properties of the mutated TRPC6 (Gigante *et al.*, 2011). A M132T mutant, for example, causes an early onset of FSGS in the childhood, which correlates with a massively increased channel activity of this mutant (Heeringa *et al.*, 2009).

TRPC6, a member of the canonical TRP channels TRPC1-TRPC7, is a Ca²⁺-permeable, but poorly selective cation channel. It is regulated in a phospholipase C-dependent manner, including a direct activation by diacylglycerols {Hofmann, 1999 8 /id}{Dietrich, 2014 14 /id}. Like TRPV1, a functional TRPC6 channel complex presumably consists of four subunits. In cells that primarily express TRPC6, four subunits assemble into a functionally active pore

complex. If co-expressed with TRPC3 or TRPC7, heteromeric TRPC6-bearing channels complexes may form and mediate receptor-stimulated cation currents (Hofmann *et al.*, 2002). In TRPC6-linked FSGS, the autosomal dominant inheritance of the disease implies that mutated TRPC6 subunits may either form separate channel complexes, or they may oligomerise together with the gene product of the wild-type TRPC6 allele to form channel complexes that contain 1-3 mutated TRPC6 subunits.

TRPC6 is expressed in a variety of tissues and cell types, including vascular smooth muscle cells, mesangial cells and podocytes. Although the presence of TRPC6 in podocytes has been demonstrated by several groups, there is considerable variability concerning the abundance of the channel protein and the size of functional responses to TRPC6 activators (Kalwa *et al.*, 2015; Anderson *et al.*, 2014; Abkhezr *et al.*, 2015). Since dysregulation of TRPC6 expression in podocytes can occur in response to various stimuli, TRPC6 may also play a seminal role in secondary forms of FSGS. Conditions that cause TRPC6 upregulation or positively modulate its activation include puromycin treatment, hyperglycaemia, long-term administration of angiotensin II, TNF- α signaling, reperfusion injury or exposure to oxidative stress (Ilatovskaya & Staruschenko, 2015; Kim *et al.*, 2012; Abkhezr *et al.*, 2015; Wang *et al.*, 2009; Szabo *et al.*, 2015).

We have recently identified larixyl acetate as a potent and TRPC6-prevalent inhibitor (Urban *et al.*, 2016). We now investigate whether biological activity can be demonstrated on native TRPC6 channel complexes in podocytes and on TRPC6 variants carrying mutations that are linked to FSGS. In addition, to further improve the properties of the compound, we sought to replace the instable acetyl ester by a carbamate moiety. The resulting semisynthetic compound larixyl carbamate was equally potent as larixyl acetate, but its selectivity for TRPC6 versus TRPC3 was slightly enhanced. In primary podocyte cultures or in freshly isolated glomeruli, fluorometric Ca²⁺ assays failed to demonstrate functional expression of TRPC6. Applying quantitative RT-PCR and Western blot analysis, a very low abundance of TRPC6 expression was found in podocytes compared to pulmonary artery smooth muscle cells. Finally, electrophysiological recordings were applied to demonstrate TRPC6 currents in podocytes and their susceptibility to pharmacological inhibition by larixol derivatives.

Materials and Methods

Isolation and derivatisation of larixol

Isolation of larixol: larch turpentine (25 g) from *Larix decidua* (Kremer Pigmente, Aichstetten, Germany) was dissolved in 100 ml n-hexane, and 50 ml of 1 M KOH were added. The formed precipitate was filtrated off over Celite. The organic phase was washed with 1 M NaOH, dried over magnesium sulfate, and n-hexane was removed under reduced pressure. The yellow, oily residue was dissolved in 1 M KOH in EtOH (300 ml) and refluxed for 3 h. The solution was evaporated to half of its volume, 100 ml of water were added, and the solution was evaporated to an oily residue. To the latter, diethyl ether (100 ml) was added. The aqueous phase was separated and extracted with diethyl ether. The combined organic phases were dried over magnesium sulfate and, after filtration, solvents were removed yielding after crystallization from cyclohexane (30 ml) 2.99 g of larixol.

Larixol derivatives were prepared according to the following protocols. All compounds were purified by chromatography on silica to >95%. Purity was determined by TLC, NMR spectroscopy and for the larixyl-6-carbamate, -formate and methyl ether by elemental analysis. NMR data were assigned by using 2D experiments, namely H,H-COSY, HSQC, and HMBC experiments.

Larixyl-diacetate: Larixol (50 mg, 0.16 mmol, 1.0 equiv.) was dissolved under nitrogen in dimethylaniline (1.5 ml), and acetyl chloride (50 μ l, 0.65 mmol, 4.0 equiv.) was added. The solution was stirred at room temperature, and further acetyl chloride (25 μ l) was added after 2 h and 4 h. After 16 h, further dimethylaniline (1 ml) and acetyl chloride (25 μ l) were added, and the mixture was heated to 90°C for 3 h. The reaction was quenched by addition of water, extracted with dichloromethane, washed with saturated sodium bicarbonate solution, dried over magnesium sulfate, and the solvent was removed at reduced pressure. The obtained remainder was purified by chromatography on silica (n-hexane: ethyl acetate 95:5 \rightarrow 90:10 (v:v)), yielding 29.7 mg (48%) of the diacetate product. $R_f = 0.64$ (n-hexane: ethyl acetate 4:1 (v:v)). $^1\text{H-NMR}$ (300 MHz, CDCl_3) δ [ppm] = 0.74 (s, 3H, 20- CH_3), 0.87 (s, 3H, 18/19- CH_3), 1.01 (s, 3H, 18/19- CH_3), 1.01-1.56 (m, 12H), 1.52 (s, 3H, 16- CH_3), 1.41 (d, $J = 12$ Hz, 1H, 5-CH), 2.01 (s, 3H, Ac- CH_3), 2.03 (s, 3H, Ac- CH_3) 2.68 (dd, $J = 12$ Hz, 6 Hz, 1H, 7-CH), 4.62 (m, 1H, CH_2), 4.92 (m, 1H, CH_2), 5.03 (dt, $J = 12$ Hz, 6 Hz, 1H, 6-CH) 5.10

(s,1H), 5.14 (m, 1H), 5.96 (dd, J = 18 Hz, 12 Hz, 1H, 14-CH); $^{13}\text{C-NMR}$ (75 MHz, CDCl_3) δ [ppm] = 16.2 (20- CH_3), 17.9 (11- CH_2), 19.3 (2- CH_2), 22.2 (Ac- CH_3), 22.4 (Ac- CH_3), 22.7 (18/19- CH_3), 23.8 (16- CH_3), 33.7 (4-C), 36.4 (18/19- CH_3), 39.2 (1- CH_2), 39.4 (10-CH), 40.1 (12- CH_2), 43.7 (3- CH_2), 44.4 (7- CH_2), 56.5 (9-CH), 57.8 (5-CH), 73.5 (6-CH), 83.5 (13-C), 109.7 (17- CH_2), 113.4 (15- CH_2), 142.0 (14-CH), 145.4 (8-C), 170.2 (Ac-CO), 170.3 (Ac-CO). HRMS [$\text{M}+\text{Na}^+$] 413.26678, found: 413.26623 m/z.

Larixyl-6-propionate: Larixol (50 mg, 0.16 mmol, 1 equiv.) was dissolved under nitrogen in dichloromethane (3 ml), and the solution was cooled to 0°C. After addition of propionyl chloride (20 μl , 0.24 mmol, 1.5 equiv.) and diisopropylethyl amine (100 μl), the reaction was allowed to proceed at room temperature under stirring for 16 h. The reaction was quenched by addition of water, and the mixture was extracted with diethyl ether. Combined organic phases were washed with 1 M HCl, saturated bicarbonate solution and brine, and dried over magnesium sulfate. After filtration, solvents were removed and the product was purified by silica chromatography (n-hexane: ethyl acetate 9:1 (v:v)), yielding 23.8 mg (41%) of the larixyl-6-propionate. R_f = 0.46 (hexane: EE 9:1 (v:v)). $^1\text{H-NMR}$ (300 MHz, CDCl_3) δ [ppm] = 0.74 (s, 3H, 20- CH_3), 0.86 (s, 3H, 18/19- CH_3), 1.00 (s, 3H, 18/19- CH_3), 1.03-2.00 (m), 1.13 (t, J = 6 Hz, 3H, propionyl- CH_3) 1.27 (s, 3H, 16- CH_3), 1.40 (d, J = 12 Hz, 1H, 5-CH), 2.01 (m, 1H, 7- CH_2), 2.28 (dq, J = 6 Hz, 3 Hz, 2H, propionyl- CH_2) 2.66 (dd, J = 12 Hz, 6 Hz, 1H, 7-CH), 4.63 (s, 1H, 17- CH_2), 4.77 (s, 1H, 17- CH_2), 4.97-5.06 (m, 2H, 15- CH_2 , 6-CH), 5.20 (dd, J = 18 Hz, 1H, 15- CH_2), 5.90 (dd, J = 18 Hz, 12 Hz, 1H, 14-CH); $^{13}\text{C-NMR}$ (75 MHz, CDCl_3) δ [ppm] = 9.3 (propionyl- CH_3), 16.2 (20- CH_3), 18.2 (11- CH_2), 19.2 (2- CH_2), 22.2 (18/19- CH_3), 28.0 (16- CH_3), 28.6 (propionyl- CH_2), 33.3 (4-C), 36.4 (18/19- CH_3), 39.4 (1- CH_2), 40.1 (10-CH), 41.6 (12- CH_2), 43.7 (3- CH_2), 44.4 (7- CH_2), 56.6 (9-CH), 57.8 (5-CH), 73.3 (6-CH), 73.8 (13-C), 109.7 (17- CH_2), 112.0 (15- CH_2), 144.6 (14-CH), 145.4 (8-C), 173.7 (propionyl-CO); HRMS [$\text{M}+\text{Na}^+$] 385.2719, found: 385.27132 m/z.

The same protocol furnished 4.6 mg (7%) of the dipropionate. R_f = 0.60 (n-hexane: ethyl acetate 9:1 (v:v)). $^1\text{H-NMR}$ (300 MHz, CDCl_3) δ [ppm] = 0.74 (s, 3H, 20- CH_3), 0.87 (s, 3H, 18/19- CH_3), 1.01 (s, 3H, 18/19- CH_3), 1.01-1.56 (m, 12H), 1.13 (m, 6H, 2 x propionyl- CH_3), 1.52 (s, 3H, 16- CH_3), 1.41 (d, J = 12 Hz, 1H, 5-CH), 2.25-2.35 (m, 4H, 2 x propionyl- CH_2), 2.68 (dd, J = 12 Hz, 6 Hz, 1H, 7-CH), 4.60 (m, 1H), 4.93 (m, 1H) 5.00-5.16 (m, 3H), 5.96 (dd, J = 18 Hz, 12 Hz, 1H, 14-CH); $^{13}\text{C-NMR}$ (75 MHz, CDCl_3) δ [ppm] = 8.0 (propionyl- CH_3),

8.3 (propionyl-CH₃), 16.7, 18.0, 21.4, 22.6, 27.4, 27.6, 28.3, 28.7, 35.2, 38.0, 38.2, 38.8, 42.4, 43.2, 55.3, 56.5, 72.0 (6-CH), 81.9 (13-C), 109.4 (17-CH₂), 112.1 (15-CH₂), 140.9 (14-CH), 143.3 (8-C), 172.3 (propionyl-CO), 172.5 (propionyl-CO); HRMS [M+Na⁺] 441.29808, found: 441.29753 m/z.

Larixyl-6-carbamate: Larixol (200 mg, 0.653 mmol, 1.0 equiv.) was dissolved in dichloromethane (3 ml), 2,2,2-trichloroacetyl isocyanate (78 μ l, 0.653 mmol, 1.0 equiv.) was added and stirred at room temperature for 1 h. Then, the solvents were removed with a rotary evaporator and the dry product was dissolved in methanol (3 ml). Potassium carbonate was added (97 mg, 0.702 mmol, 1.08 equiv.) and the suspension was stirred at room temperature for 1 h. Again, the reaction mixture was evaporated to dryness. The remainder was suspended in 5 ml water, and extracted three times with diethyl ether (10 ml each). Combined organic phases were washed twice with water and once with brine, dried over sodium sulfate, and evaporated to dryness. The solid remainder was purified by flash chromatography over silica with ethyl acetate /n-hexane 1:1 as eluent, furnishing the product as a white powder (167 mg, 73% yield). Mp: 122°C. R_f = 0.52 (n-hexane: ethyl acetate 1:1 (v:v)); ¹H NMR (500 MHz, CDCl₃) δ [ppm] = 0.73 (s, 3H, 20-CH₃), 0.91 (s, 3H, 18/19-CH₃), 0.99 (s, 3H, 18/19-CH₃), 1.00-1.08 (m, 1H, 12-CH₂), 1.18-1.38 (m, 8H), 1.41-1.62 (m, 5H), 1.69-1.78 (m, 2H), 1.99-2.08 (m, 1H, 7-CH₂), 2.71 (dd, J = 12.3 Hz, 5.2 Hz, 1H, 7-CH₂), 4.62 (q, J = 1.6 Hz, 1H, 17-CH₂), 4.67 (s, 2H, OCONH₂), 4.87-4.94 (m, 2H, 17-CH₂, H-6), 5.04 (dd, J = 10.8 Hz, 1.2 Hz, 1H, 15-CH₂), 5.19 (dd, J = 17.4 Hz, 1.3 Hz, 1H, 15-CH₂), 5.89 (dd, J = 17.4 Hz, 10.8 Hz, 1H, H-14); ¹³C NMR (126 MHz, CDCl₃) δ 16.04 (20-CH₃), 18.10, 19.16, 22.51 (18/19-CH₃), 27.78, 33.65, 36.31 (18/19-CH₃), 39.24 (12-CH₂), 39.90 (10-CH), 41.42, 43.67, 44.68, 56.45, 57.97, 73.58 (C-13), 74.17 (6-CH), 109.51 (17-CH₂), 111.77 (15-CH₂), 144.47 (C-8), 145.28 (14-CH), 156.10 (C=O); HRMS [M+Na⁺] 372.251, found: 372.253 m/z; Anal. Calcd for C₂₁H₃₅NO₃: C, 72.17; H, 10.09; N, 4.01; Found: C, 71.54; H, 9.858; N, 3.864.

Larixyl-6-formate: Larixol (50 mg, 0.16 mmol, 1.0 equiv.) was dissolved in dry dichloromethane (5 ml), formic acid (13 μ L, 0.326 mmol, 2.0 equiv.) and DMAP (2 mg, 0.016 mmol, 0.1 equiv.) was added. The solution was cooled to 0°C, DCC (44 mg, 0.21 mmol, 1.3 equiv.) was added and the solution was stirred for 15 min at 0°C. Thereafter, the icebath was removed and the reaction stirred overnight at room temperature. The precipitated urea

was filtered off, washed with DCM and the filtrate evaporated under reduced pressure. The obtained remainder was purified by flash chromatography on silica (n-hexane: 85:15 (v:v)), yielding 48 mg (88%) of the larixyl-6-formate as white crystals. Mp. 90 °C. R_f = 0.48 (n-hexane: ethyl acetate 3:1 (v:v)). $^1\text{H-NMR}$ (700 MHz, CDCl_3) δ [ppm] = 0.77 (d, J = 0.7 Hz, 3H, 20- CH_3), 0.91 (s, 3H, 18/19- CH_3), 1.06 (s, 3H, 18/19- CH_3), 1.09 (td, J = 12.9 Hz, 4.2 Hz, 1H), 1.24 – 1.33 (m, 5H), 1.34 – 1.42 (m, 3H), 1.47 – 1.52 (m, 2H), 1.53 – 1.63 (m, 2H), 1.63 – 1.66 (m, 1H), 1.74 – 1.80 (m, 2H), 2.09 – 2.15 (m, 1H, 7- CH_2), 2.73 (dd, J = 12.3 Hz, 5.1 Hz, 1H, 7- CH_2), 4.69 (d, J = 1.6 Hz, 1H, 17- CH_2), 4.97 (d, J = 1.6 Hz, 1H, 17- CH_2), 5.08 (dd, J = 10.8 Hz, 1.2 Hz, 1H, 15- CH_2), 5.16 – 5.21 (m, 1H, H-6), 5.22 (dd, J = 17.4 Hz, 1.2 Hz, 1H, 15- CH_2), 5.93 (dd, J = 17.4 Hz, 10.8 Hz, 1H, H-14), 8.10 (d, J = 0.9 Hz, 1H, COH); $^{13}\text{C-NMR}$ (176 MHz, CDCl_3) δ 15.93 (20- CH_3), 18.01, 18.97, 22.37 (18/19- CH_3), 27.80 (16- CH_3), 33.70, 36.31 (18/19- CH_3), 39.10, 39.93, 41.27, 43.50, 44.24, 56.32, 57.47 (9-CH), 73.30 (5-CH), 73.33 (C-6), 73.46 (C-13), 109.85 (17- CH_2), 111.72 (15- CH_2), 144.02 (8-C), 145.14 (14-CH), 160.64 (CHO); HRMS [$\text{M}+\text{Na}^+$] 357.24, found: 357.242 m/z; Anal. Calcd for $\text{C}_{21}\text{H}_{34}\text{O}_3$: C, 75.41; H, 10.25; Found: C, 75.43; H, 9.66.

Larixyl-6-phenylacetate: Larixol (50 mg, 0.16 mmol, 1.0 equiv.) was dissolved in dry dichloromethane (3 mL), phenylacetic acid (33 mg, 0.245 mmol, 1.5 equiv.) and DCC (50 mg, 0.245 mmol, 1.5 equiv.) was added. After 5 min, DMAP (4 mg, 0.032 mmol, 0.2 equiv.) was added and the solution was stirred overnight at room temperature. The precipitated urea was filtered off, washed with DCM and the organic phase extracted with 15 mL NaHCO_3 . The organic phase was dried over MgSO_4 and evaporated under reduced pressure. The product was purified by flash chromatography on silica (n-hexane: ethyl acetate 85:15 (v:v)), yielding 37 mg (53%) of the larixyl-6-phenylacetate as colorless oil. R_f = 0.52 (n-hexane: ethyl acetate 3:1 (v:v)). $^1\text{H-NMR}$ (700 MHz, CDCl_3) δ [ppm] = 0.75 (s, 3H, 20- CH_3), 0.87 (s, 3H, 18/19- CH_3), 0.98 (s, 3H, 18/19- CH_3), 1.07 (td, J = 12.7 Hz, 4.1 Hz, 1H, 12- CH_2), 1.22 – 1.32 (m, 5H), 1.32 – 1.41 (m, 3H), 1.44 (d, J = 11.3 Hz, 1H, H-5), 1.46 – 1.51 (m, 1H), 1.52 – 1.64 (m, 4H), 1.72 – 1.79 (m, 2H), 1.96 – 2.02 (m, 1H, 7- CH_2), 2.66 (dd, J = 12.3 Hz, 5.1 Hz,

1H, 7-CH₂), 3.57 – 3.66 (m, 2H, CH₂-Ph), 4.65 (d, J = 1.6 Hz, 1H, 17-CH₂), 4.92 (d, J = 1.7 Hz, 1H, 17-CH₂), 5.03 – 5.12 (m, 2H, 15-CH₂, H-6), 5.22 (dd, J = 17.3 Hz, 1.2 Hz, 1H, 15-CH₂), 5.92 (dd, J = 17.3 Hz, 10.8 Hz, 1H, H-14), 7.26 – 7.32 (m, 3H, Ph), 7.32 – 7.36 (m, 2H, Ph); ¹³C-NMR (176 MHz, CDCl₃) δ 15.99 (20-CH₃), 18.01, 19.01, 22.45 (18/19-CH₃), 27.74 (16-CH₃), 33.51, 36.15 (18/19-CH₃), 39.13 (12-CH₂), 39.89 (10-CH), 41.30, 42.28, 43.45, 43.96 (7-CH₂), 56.36 (9-CH), 57.45 (5-CH), 73.48 (C-13), 73.88 (6-CH), 109.56 (17-CH₂), 111.69 (15-CH₂), 127.01 (Ph-C-4), 128.50 (Ph-C-3/3'), 129.29 (Ph-C-2/2'), 133.95 (Ph-C-1), 144.24 (C-8), 145.16 (C-14), 170.64 (C=O); HRMS [M+Na⁺] 447.28, found 447.287 m/z;

Larixyl-6-methylether: Larixol (113 mg, 0.367 mmol, 1.0 equiv.) was dissolved in dry tetrahydrofuran (3 ml) and cooled to 0°C. Then sodium hydride (29 mg, 60% suspension in mineral oil, 0.735 mmol, 2.0 equiv.) was added and the solution stirred for 5 min, followed by the addition of iodomethane (69 µL, 1.10 mmol, 3.0 equiv.). After 5 min, the icebath was removed and the reaction stirred overnight at room temperature. Additional 20 mg sodium hydride (20 mg) and iodomethane (69 µL) was added and stirred for additional 24h. The solvent was evaporated under reduced pressure. The obtained remainder was suspended in dichloromethane and extracted with water (15 mL). The organic phase was dried over MgSO₄ and evaporated under reduced pressure. The product was purified by flash chromatography over silica (n-hexane: ethyl acetate 85:15 (v:v)), yielding 42 mg (36%) of a 62:38 (determined by NMR integration) mixture of larixyl-6-methylether (A) and larixyl-16-methylether (B) as colorless crystals. R_f = 0.4 (n-hexane: ethyl acetate 4:1 (v:v)). ¹H NMR (700 MHz, CDCl₃) δ [ppm] = 0.70 – 0.72 (m, 5H, 20-CH₃ of A+B), 0.94 (s, 3H, 18/19-CH₃ of A), 1.03 (s, 2H, 18/19-CH₃ of B), 1.06 (td, J = 12.7, 4.0 Hz, 2H, 12-CH₂ of A+B), 1.10 – 1.14 (m, 4H), 1.18 (s, 2H, 18/19-CH₃ of B), 1.23 – 1.41 (m, 1H), 1.44 – 1.52 (m, 2H), 1.52 – 1.63 (m, 4H), 1.71 – 1.81 (m, 3H), 1.88 – 1.95 (m, 1H, 12-CH₂ of A), 2.06 (td, J = 11.5 Hz, 10.6, 1.8 Hz, 0.6 H, 12-CH₂ of B), 2.69 (dd, J = 12.2 Hz, 4.9 Hz, 0.6H, 12-CH₂ of B), 2.86 (dd, J = 12.2 Hz, 4.7 Hz, 1H, 12-CH₂ of A), 3.15 (s, 2H, OCH₃ of B), 3.26 (td, J = 10.6 Hz, 4.7 Hz, 1H, H-6 of A), 3.34 (s, 3H, OCH₃ of A), 3.84 (td, J = 10.7 Hz, 4.9 Hz, 0.6H, H-6 of B), 4.60 (q, J =

1.6 Hz, 0.6H, 17-CH₂ of B), 4.62 (q, J = 1.6 Hz, 1H, 17-CH₂ of A), 4.89 (q, J = 1.6 Hz, 0.6H, 17-CH₂ of B), 4.91 (q, J = 1.6 Hz, 1H, 17-CH₂ of A), 5.07 (dd, J = 10.8 Hz, 1.2 Hz, 1H, 15-CH₂ of A), 5.13 (dd, J = 17.7 Hz, 1.3 Hz, 0.6H, 15-CH₂ of B), 5.18 (dd, J = 10.9 Hz, 1.3 Hz, 0.6H, 15-CH₂ of B), 5.22 (dd, J = 17.4, 1.3 Hz, 1H, 15-CH₂ of A), 5.76 (dd, J = 17.7, 11.0 Hz, 0.6H, H-14 of B), 5.93 (dd, J = 17.4 Hz, 10.8 Hz, 1H, H-14 of A); ¹³C NMR (176 MHz, CDCl₃) δ [ppm] = 16.08 (20-CH₃ of B), 16.29 (20-CH₃ of A), 17.70, 18.10, 19.14, 21.61, 22.38, 22.66, 27.82, 29.71, 33.82, 33.90, 36.46, 36.66, 38.50, 39.32, 39.41, 39.56, 41.40, 43.25 (7-CH₂ of A), 43.66, 43.79, 49.23 (7-CH₂ of B), 50.07 (OCH₃ of B), 55.76, 56.60, 56.75, 58.91 (OCH₃ of A), 60.59, 71.71 (C-6 of A), 73.53, 77.56, 80.76 (C-6 of B), 108.21 (17-CH₂ of A), 108.27 (17-CH₂ of B), 111.62 (15-CH₂ of A), 114.63 (15-CH₂ of B), 143.03 (14-CH of A), 145.21 (14-CH of B), 145.70 (C-8 of B), 145.78 (C-8 of A); HRMS [M+Na⁺] 343.26, found: 343.265 m/z; Anal. Calcd for C₂₁H₃₆O₂: C, 78.70; H, 11.32; Found: C, 78.78; H, 11.44.

Mutagenesis of human TRPC6

To obtain pcDNA3-based expression plasmids, encoding FSGS-related point-mutated TRPC6, site-directed mutagenesis of human TRPC6-YFP was performed with the QuikChange kit (Agilent Technologies, Santa Clara, CA, USA), following the manufacturer's recommendations and applying suitable forward and reverse primers (sequences are provided in Supplementary Table 1). After PCR, mutated plasmids were transformed in XL2-Blue competent cells. Clones were selected, and the mutation was verified by cDNA sequencing.

Cell culture and transfection of HEK293 cells

HEK293 cells were cultured in Earle's Minimum Essential Medium (MEM; Sigma, Munich, Germany), supplemented with 10% fetal calf serum (Gibco Thermo Fisher Scientific, Darmstadt, Germany), 2 mM L-glutamine, 100 U/ml penicillin, and 0.1 mg/ml streptomycin. To characterize human TRPC6 mutants and to verify the efficiency of larixol derivatives, parental HEK293 cells were seeded on 25-mm glass coverslips, and transfected with 4 µl Fugene HD (Promega, Mannheim, Germany) and 2 µg of DNA encoding wild-type or

mutated variants of TRPC6-YFP. For FRET assays, HEK293 cells were co-transfected with 0.5-0.8 µg pcDNA3-hTRPC6-CFP wild-type and 1.2-1.5 µg pcDNA3-hTRPC6-YFP mutant to achieve a 1:1 molar ratio between YFP- and CFP-fused channel constructs. After 24 hours, cells were directly used for $[Ca^{2+}]_i$ imaging and FRET measurements, or singularised with 0.25% trypsin for electrophysiological experiments. Fluorescence plate imaging analyses of cells expressing TRPC6 mutants were realized with stably transfected polyclonal cell lines, selected by adding 1 mg/ml geneticin (G418) to the medium. All cells were maintained at 37°C and in a 5% CO₂-aerated, humidified atmosphere.

Isolation of glomeruli and podocyte primary cultures

Kidneys were isolated by dorsal dissection from 10-days-old (P10) or 8-week-old Wistar rats or from 3- to 4-week-old mice. Mouse strains were C57BL/6J or B6.Cg-Tg(NPHS2-Trpc6) F419Walz/J transgenic mice intercrossed on C57BL/6J background, purchased via Charles River Laboratories from The Jackson Laboratory (Bar Harbor, MA, USA; Stock number 018293). After removing the fibrous renal capsule, cortical tissue was obtained, cut in small pieces and washed in ice-cold buffer, containing 127 mM NaCl, 5.9 mM KCl, 1.2 mM MgCl₂, 1.8 mM glucose, and 10 mM HEPES adjusted to pH 7.4. Then, the collected tissue was enzymatically digested for 12-15 minutes at 37°C in the same buffer, additionally containing 0.75 mg/ml collagenase (Sigma), 50 µM CaCl₂ and 0.5% bovine serum albumin. The digested tissue was recovered by short centrifugation, and resuspended in a podocyte culture medium, containing RPMI 1640 supplemented with 10% fetal calf serum, 2 mM L-glutamine, 100 U/ml penicillin, and 0.1 mg/ml streptomycin. The suspension, which contained decapsulated glomeruli, was repeatedly sieved through cell strainers (Greiner) with decreasing pore sizes (100 µm, 70 µm and 40 µm). Glomeruli-enriched fractions were obtained by turning and rinsing the sieve size 70 µm (adult rat) or 40 µm (P10 rats and mice) with medium. For Ca²⁺ measurements, isolated glomeruli were directly loaded with 5 µM fura-2/AM (AAT Bioquest, Hamburg, Germany) or 4 µM fluo-4/AM (Invitrogen, Karlsruhe, Germany) in podocyte culture medium for 30 min at 37°C, centrifuged (100 x g; 5 min) and measured 30 min after allowing glomeruli to settle in collagen-coated 24-well cell culture plates or pigmented clear-bottom 384-well plates (Corning, Kaiserslautern, Germany) in HBS containing 0.1% BSA. In case of isolation of primary podocyte cultures, glomeruli suspended

in podocyte culture medium were seeded into 24-well plates which were freshly coated with collagen A (Biochrom, Berlin, Germany) or into collagen type I-coated 60-mm dishes (Greiner, Frickenhausen, Germany). Analyses were done 5 to 8 days after growing out of podocytes from the glomeruli. The fraction of cells with cobblestone-like morphology was over 80%.

PASMC isolation

Pulmonary artery smooth muscle cells (PASMC) were obtained from 3-week-old Wistar rats or from 3- to 4-week old mice, following a previously described procedure (Urban *et al.*, 2016). PASMC were cultured for 1 to 2 weeks in DMEM/Ham's F12 medium (1:1 vol/vol), supplemented with 10% fetal calf serum, 2 mM L-glutamine, 2.7 g/l D-glucose, 25 mM HEPES, 100 U/ml penicillin, and 0.1 mg/ml streptomycin before preparation of RNA was done. For protein expression analysis, functional TRPC6 $[Ca^{2+}]_i$ imaging and membrane potential measurements, PASMC were used up to the seventh passage.

Ca²⁺ measurements in multiwell plates

Fluorometric Ca²⁺ assays in HEK293 cell lines and glomeruli were done in HEPES-buffered saline (HBS), containing 132 mM NaCl, 6 mM KCl, 1 mM MgCl₂, 1mM CaCl₂, 5.5 mM D-glucose, and 10 mM HEPES, 0.03% bovine serum albumin (BSA) adjusted to pH 7.4 with NaOH. Isolated glomeruli or trypsin-detached HEK293 cell lines were loaded with 4 μM fluo-4/AM (Invitrogen) in culture medium for 30 min at 37°C. After centrifugation (100 x g; 3 min), glomeruli and HEK293 cells were resuspended in HBS and dispensed into pigmented clear-bottom 384-well plates (Corning, USA). Fluorescence signals were recorded in a custom-made fluorescence imaging plate reader (FLIPR) built into a robotic liquid handling station (Freedom Evo 150, Tecan, Männedorf, Switzerland) as described (Urban *et al.*, 2016). First TRPC6 inhibitors were added to stably transfected HEK293 cells at the indicated final concentrations, and incubated for 5 min. Then, cells were stimulated with 50 μM OAG during continuous fluorescence recording, controlled by a Micromanager software (Edelstein *et al.*, 2010). Fluorescence intensities were calculated from image stacks for each well with ImageJ (Abramoff & Magalhaes, 2004), corrected for background signals and normalized to the initial intensities (F/F₀). Concentration response curves were generated by fitting the data to

Hill equations. If freshly isolated glomeruli were examined, larixyl carbamate was incubated for 10 min, and TRPC6 activation was indirectly triggered with 10 μM angiotensin II.

Microfluorometric $[\text{Ca}^{2+}]_i$ imaging analysis

Transfected HEK293 cells or PASMC grown on 24-mm coverslips or primary podocyte cultures grown in 24-well plates were loaded with 4 μM fura-2/AM (AAT Bioquest) in HBS containing 0.2% BSA for 30 min at 37°C. After washing cells, podocytes and PASMC were allowed to equilibrate in HBS containing 0.1% BSA and 1 μM bisindolylmaleimide 1 (BIM) to prevent activation of protein kinase C. HEK293 cells on coverslips were mounted in a bath chamber and superfused with HBS containing 0.1% BSA. $[\text{Ca}^{2+}]_i$ measurements were performed on an inverted epifluorescence microscope with a Fluar 10x/0.5 objective (Carl Zeiss, Jena, Germany) and calibrated as described (Urban *et al.*, 2016; Lenz *et al.*, 2002). Heterologously expressed TRPC6 in HEK293 cells was either activated with 50 μM OAG or indirectly stimulated by challenging cells with a mixture of 1 mM carbachol, 300 μM ATP and 0.5 units/ml thrombin after internal Ca^{2+} store depletion with 2 μM thapsigargin. To evaluate the inhibitory potency of new TRPC6 blockers, HEK293 cells were pretreated with 1 μM of respective compound. Activation of endogenous TRPC6 in PASMC, podocytes or freshly isolated glomeruli was attempted with 100 μM OAG, 20 μM GSK1702934A, 10 μM angiotensin II, 100 μM ATP, 10 μM bradykinin, 100 μM carbachol or 0.5 units/ml thrombin. In some experiments, Ca^{2+} mobilisation from the endoplasmic reticulum was abrogated by adding 2 μM thapsigargin to the bath 5 min before application of the respective agonists.

Fluorescence resonance energy transfer (FRET) measurements

FRET was assessed and quantified by measuring donor (TRPC6-CFP) unquenching during selective photobleaching of the FRET acceptor (YFP fused to the C terminus of wild-type or mutant TRPC6) essentially as described earlier (Hellwig *et al.*, 2005). To account for the expected 1:1 gene dose in FSGS patients, the molar ratio between co-expressed CFP- and YFP-tagged TRPC6 constructs was determined as described, and adjusted to achieve only a slight (10-30%) excess of the YFP-fused FRET acceptor over the co-expressed CFP-fused donor.

Genotyping and quantitative RT-PCR

After reproduction of B6.Cg-Tg(NPHS2-Trpc6) F419Walz/J transgenic mice, genotyping of 2 week old littermates was performed, applying a REDExtract-N-Amp Tissue PCR Kit (Sigma), a Trpc6 exon 8 forward primer 5'-gacactgttctgggctatct and a Trpc6 3' UTR reverse primer 5'-cagtgtgatggagctcga as reported (Krall *et al.*, 2010). As an internal control, the endogenous Trpc6 gene was amplified, using a Trpc6 intron 8 reverse primer 5'-cccatttcctctcccaaa. Amplicons were detected in gel electrophoresis as 830 bp product (transgene), and 530 bp (endogenous TRPC6) bands, respectively.

To quantify the TRPC6 transcript abundance, total RNA was isolated from primary podocytes and PASMC with a Trizol reagent (VWR Life Science, Erlangen, Germany). First strand cDNA was synthesized from RNA templates with a RevertAid first strand cDNA synthesis kit (Thermo Scientific) and random hexamer primers, following the manufacturer's instructions. Finally, cDNA was applied directly as template in real-time PCR using DyNAmo ColorFlash SYBR Green qPCR Kit and a Piko Real 24 thermocycler (Thermo Scientific). Primers for detecting native TRPC6 and smooth muscle α -actin transcripts were independently designed for rat and mouse TRPC6. For quantitative RT-PCR analysis of podocin expression, common mouse/rat primers were used. Transgenic TRPC6 RNA was detected with a Jackson Laboratory genotyping primer and a reverse hemagglutinin (HA) tag primer. PCR was performed with a three-step protocol (7 min at 95°C; and 45 cycles of 15 s at 95°C, 20 s at 56°C/ 63°C/ 66°C, 30s at 72°C; final extension of 2 min at 72°). Results were normalized to 18s RNA, using the ΔC_T method (ratio reference/target = $2^{C_T(\text{reference}) - C_T(\text{target})}$). All applied primers are listed in the Supplementary Table 1.

Western blot and immunofluorescence analysis

Cultured podocytes and PASMC were washed twice with PBS, harvested with a cell scraper and homogenized with a RIPA buffer, containing 150 mM NaCl, 50 mM Tris-HCl pH 7.4, 1 mM EDTA, 1% NP-40, 0.25% natrium deoxycholate, 1 mM NaF, 1 mM natrium orthovanadate, 1 mM PMSF, 1 μ g/ml aprotinine, 1 μ g/ml leupeptine, and 1 μ g/ml pepstatin. Homogenisation of glomeruli in RIPA was done directly after isolation and two washing steps with PBS. To assess protein yield of the samples, a BCA protein assay was used (Thermo Fisher Scientific). Then, 30 μ g protein of glomeruli or HEK293 cells, and 18 μ g protein of

podocytes or PASMC were lysed in Laemmli buffer, and subjected to SDS-PAGE (8% acrylamide/bis-acrylamide). Separated proteins were electroblotted onto PVDF membranes. Membranes were blocked for 30 min in 5% nonfat dry milk TBST (20 mM Tris pH 7.4, 137 mM NaCl, 0.1% Tween-20) and incubated overnight with anti-TRPC6 (Alomone, Jerusalem, Israel; 1:200), anti-podocin (Sigma; 1:2,000) or anti- α smooth muscle actin (α -SMA) (Sigma; 1:1,000) antibodies in TBS, 1% dry milk, 0.5% Tween-20. As a housekeeping protein, GAPDH was analysed by 2 hours incubation with anti-GAPDH (Millipore, Darmstadt, Germany; 1:5,000) or anti- β -actin (Sigma; 1:5,000). Same-day or next day, membranes were washed, followed by incubation with secondary peroxidase-coupled anti-rabbit (TRPC6, podocin, GAPDH) or anti-mouse (α -SMA, β -actin) antibodies (Sigma; 1:5,000) for 2 hours. Peroxidase activity was detected using a Novex ECL chemiluminescence reagent (Invitrogen). For TRPC6 analysis, a more sensitive peroxidase substrate SuperSignal West Femto (Thermo Fisher Scientific) was necessary. Between detecting the different target proteins, the PVDF membranes were stripped with a 1 M glycine solution adjusted to pH 1.8 with HCl.

For immunofluorescence, freshly isolated glomeruli were transferred onto glass slides, dried quickly under a ventilator and fixed with methanol. Primary isolated podocytes were split onto freshly collagen A-coated μ slides (ibidi) for 2 days and fixed with 4% paraformaldehyde. Then, samples were blocked and permeabilized with PBS, supplemented with 3% BSA, 0.1% Triton-X100 and 10% goat serum. Primary antibody decoration of slides was followed overnight with polyclonal rabbit anti-podocin (Sigma; 1:250) and monoclonal mouse anti- α -SMA (Sigma; 1:500). After washing slides three times for 5 minutes in PBS, bonded primary antibodies were decorated with Alexa Fluor 488-conjugated goat anti-rabbit antibody (Invitrogen A11008; 5 μ g/ml) and Cy3-conjugated donkey anti-mouse antibody (Jackson ImmunoResearch Laboratories; 1:400) for 2 hours. Finally, nuclei were counterstained with Hoechst 33258 (10 μ g/ml), slides were washed again and mounted with Mowiol 4-88 (Roth) or ibidi mounting medium (ibidi). Fluorescence detection was performed with a LSM 510 META confocal microscope (Carl Zeiss), using Plan-Apochromat 63x/1.3 or 20x/0.8 objectives.

MTT assay/ Detection of cell viability

Cell viability was assessed in parental HEK293 cells with a (3-(4,5-dimethylthiazol-2-yl)-2,5-diphenyltetrazolium bromide) (MTT) assay. Cells were seeded in poly-L-lysine-coated 96-well plates and grown for 24 hours until monolayers reached 50% confluency. Then medium was exchanged, and larixyl derivatives or the corresponding DMSO solvent controls were added and incubated for another 24 hours. After 24 hours, the medium was replaced with fresh one, but now containing 0.5 mg/ml MTT. After 3 hours of incubation, supernatants were removed, cells were lysed and formazan crystals were completely dissolved with undiluted DMSO. Finally, absorbance measurements at 560 nm and 670 nm were done with a plate reader (Polarstar Omega, BMG Labtech, Germany). The differences of both extinctions were calculated, and values were normalized to the 0.25% solvent control.

Membrane potential measurements

The determination of membrane potential changes by LC and LMA were executed in PASMIC using the fluorescence dye DiBAC₄(3). PASMIC grown on 24-mm coverslips were mounted in a bath chamber and loaded for 15 to 20 min at 37°C with 500 nM DiBAC₄(3) (AAT Bioquest) in HBS, containing 2 mM CaCl₂. DiBAC₄(3) fluorescence of PASMIC was continuously detected on an inverted microscope (Axiovert 100 with a Fluar 10x/0.5 objective, Carl Zeiss, Germany) equipped with a monochromator (Polychrome II, TILL-Photonics, Germany), and a 12-bit cooled CCD camera (Flowmaster, LaVision) by exciting the dye at 480 nm and collecting emitted light through a 512-nm long pass filter. The test compounds were added after a baseline recording of 1 minute.

Electrophysiological procedures

HEK_{hTRPC6-YFP} cells and podocytes were seeded at low density on PLL-coated glass coverslips. After 6-24 hours, TRPC6 membrane currents were recorded in the whole-cell patch clamp configuration, using a Multiclamp 700B amplifier with a Digidata 1440A digitizer controlled by the PClamp 10 software (Molecular Devices, Sunnyvale, CA, USA). Coverslips were mounted in a chamber (Warner Instruments, Hamden, CT; USA), placed onto the stage of an inverted microscope, and perfused with standard extracellular solution contained 140 mM NaCl, 5 mM CsCl, 2 mM MgCl₂, 1 mM CaCl₂, and 10 mM HEPES, 0.1% BSA adjusted to pH 7.4 with NaOH. In case of podocyte stimulation with OAG, the bath solution

additionally contained 1 μM BIM to suppress simultaneous activation of PKC. Patch pipettes were pulled from borosilicate glass capillaries BG150F-8P (Science Products) with a pipette puller PIP6 (HEKA Elektronik, Lambrecht, Germany) and had a resistance of 4-10 M Ω when filled with the standard pipette solution: 140 mM CsCl, 4 mM MgCl₂, 10 mM EGTA, and 10 mM HEPES adjusted to pH 7.2 with CsOH. In all whole-cell measurements, serial resistance was lower than 13 M Ω , and compensated by 70%. To record current/voltage (I/V) curves, voltage ramps (400 mV s⁻¹) ranging from -100 mV to +100 mV were applied. Currents were filtered at 3 kHz with a four-pole Bessel filter and sampled at 10 kHz.

Nomenclature of Targets and Ligands

Key protein targets and ligands in this article are hyperlinked to corresponding entries in <http://www.guidetopharmacology.org>, the common portal for data from the IUPHAR/BPS Guide to PHARMACOLOGY (Southan et al., 2016), and are permanently archived in the Concise Guide to PHARMACOLOGY 2015/16 (Alexander et al., 2015).

Results

Derivatisation of larixol

Since monoacetylation of larixol at its secondary alcohol was known to enhance the potency of TRPC6 inhibition in larixyl monoacetate (LMA) (Urban *et al.*, 2016), we sought to add a second acetylation at the tertiary alcohol of larixol, and/or to replace the acetate by other substituents to further improve the properties of the TRPC6-inhibiting pharmacophore. Under harsher reaction conditions, various carboxylate esters were formed, which included modification of both hydroxyl groups of larixol. Of them, larixyl diacetate and larixyl dipropionate were less potent in inhibiting wild-type TRPC6 in a stably transfected HEK_{hTRPC6-YFP} cell line than the previously characterised LMA or a larixyl mono-6-propionate (Fig. 1A-D). Despite its reasonably TRPC6-prevalent mode of action, higher IC₅₀ values argued against a favourable modification at the tertiary alcohol of the 3-hydroxy-3-methylpent-4-enyl group of larixol. Instead, we modified the hydroxyl group at the C6 atom of the diterpene ring. Here, the addition of a methyl ether, or of formyl or propionyl groups did not significantly improve the potency of TRPC6 inhibition compared to LMA. Likewise, the selectivity to prevent the OAG-induced activation of TRPC6 compared to the activation of stably transfected TRPC3 or TRPC7 was similar or lower than that of LMA. Of note, larixyl methyl ether, larixyl formate, LMA, and larixyl propionate elicited a concentration-dependent

biphasic effect on TRPC7, with a slight potentiation at lower concentrations and channel inhibition at higher concentrations. With an IC_{50} of 36 μ M, a larger phenylacetate-substituted larixol was only poorly active and selective (Fig. 1H). Reasoning that the ester bond in LMA may be readily cleaved by intracellular esterases e.g. in the liver, we replaced the acetate group in LMA by a carbamate group. Larixyl carbamate (LC) displayed a favourable potency with an IC_{50} to inhibit wild-type TRPC6 of 0.48 μ M (Fig. 1C). Of note, the selectivity to inhibit TRPC6, but not TRPC3 was 30-fold and, thus, slightly higher than that of the previously reported LMA. For comparison, we assessed the inhibition of TRPC3, TRPC6 and TRPC7 by the compound SKF-96365 in the same assay. As expected, SKF-96365 was moderately potent and poorly specific. The corresponding IC_{50} values were 5.0 μ M, 7.1 μ M, and 19 μ M to inhibit TRPC6, TRPC3, and TRPC7, respectively (Fig. 1I).

To assess a potential cytotoxicity of the new larixol derivatives, we executed an MTT assay in parental HEK293 cells, applying the three highest compound concentrations used in the FLIPR analysis (Fig.1B-H). All compounds stocks were dissolved in DMSO at a concentration of 10 mM. Compared to the respective solvent control, none of the TRPC6 inhibitors significantly affected the cell viability at a concentration of 25 μ M, with the exception of larixyl diacetate (Fig.1J). Of note, LC concentrations necessary for full TRPC6 block we determined at only 5 μ M in Ca^{2+} measurements and 1 μ M in electrophysiology.

Generation and functional expression of FSGS-related TRPC6 mutants

Plasmids which encode TRPC6 constructs that carry FSGS-related point mutations were generated by site-directed mutagenesis and confirmed by cDNA sequencing. Upon transient heterologous expression in HEK293 cells, fluorometric single cell $[Ca^{2+}]_i$ analyses reproduced the gain of function phenotype in the P112Q, M132T, R175Q, and Q889K point-mutated TRPC6 constructs. Here, the basal as well as the OAG (50 μ M)-induced peak $[Ca^{2+}]_i$ were up to 3-fold higher than in cells expressing the wild-type TRPC6. Of the two remaining constructs, R895C and E897K, only R895C gave rise to a slightly higher basal $[Ca^{2+}]_i$, but the stimulated peak $[Ca^{2+}]_i$ displayed only a statistically not significant trend to higher values (Table 1).

Since TRPC6-linked FSGS is an autosomal dominant inheritable disease, patients have a second allele, which encodes wild-type TRPC6. Using fluorescence resonance energy transfer (FRET) analyses, we tested whether YFP-fused mutated TRPC6 constructs can still form oligomeric assemblies with wild-type TRPC6, which was C-terminally fused to CFP. When transiently co-expressed with a 1.1- to 1.3-fold molar excess of YFP-fused constructs

over TRPC6-CFP, all investigated TRPC6 mutants gave rise to robust FRET signals, ranging from FRET efficiencies of 15.9% to 19.7%. Under the same experimental conditions, the wild-type TRPC6-CFP:TRPC6-YFP complex developed a FRET coupling efficiency of 18.0%. From these data, we conclude that all investigated TRPC6 mutations are still capable of forming channel complexes together with TRPC6 subunits that are encoded by the wild-type allele (Table 2).

Inhibition of Ca²⁺ entry through FSGS-mutated TRPC6 by larixol derivatives

The efficiency of LMA to inhibit wild-type or mutated TRPC6 in a GPCR-mediated activation mode was tested by calibrated single-cell [Ca²⁺]_i analysis in fura-2-loaded HEK293 cells, which were transiently transfected to express wild-type TRPC6 or FSGS-related mutant TRPC6 variants. Cells grown on glass coverslips were mounted into bath chambers, exposed to HBS, containing either 1 μM LMA or the solvent, and then incubated with 2 μM thapsigargin for 5 min to deplete inositol 1,4,5-trisphosphate-sensitive Ca²⁺ stores. Thereafter, an agonist mix, comprising maximally effective concentrations of ATP (300 μM), carbachol (1 mM), and thrombin (0.5 units/ml) was added to the bath to activate G-protein-sensitive phospholipases C and, in turn, TRPC6. Irrespective of the expression of wild-type or mutated TRPC6 variants, [Ca²⁺]_i signals that were elicited by the agonist mix were strongly and significantly attenuated if cells were pretreated with 1 μM LMA (Fig. 2). When compared the findings in the OAG-activated mode (see Table 1), the relative order of channel hyperactivity was similar with P112Q, M132T, R175Q and Q889K mutants causing the strongest enhancement of signals compared to wild-type TRPC6 or the R895C and E897K mutants. Of note, the elevated basal [Ca²⁺]_i in cells overexpressing the M132T variant (Fig. 2C) was efficiently lowered in the presence of 1 μM LMA. A remaining, small [Ca²⁺]_i signal seen in LMA-treated cells expressing the P112Q, M132T, or R175Q variants may either indicate partial inhibition of the channel or an incomplete store depletion.

To quantitatively assess the potency of inhibition of FSGS-related TRPC6 variants by LMA and by the newly synthesized LC, we generated stably transfected cell lines for each of the six TRPC6 channel mutants, and applied a semi-quantitative multiwell Ca²⁺ analysis in fluo-4-loaded cell suspensions. Here, a complete inhibition of OAG (50 μM)-induced Ca²⁺ signals was seen in cells pretreated with 7.5-15 μM of either LMA or LC. Concentration response curves obtained by applying various concentrations of LMA or LC revealed IC₅₀ values of 0.35-0.65 μM LMA for most TRPC6 constructs. The R175Q mutant appeared to be inhibited with a slightly lower potency (IC₅₀ = 0.91 μM). Applying LC as the TRPC6 inhibitor, we

obtained very similar results with IC_{50} values of 0.41-0.66 μM for five TRPC6 variants, and 1.03 μM for the R175Q construct (Fig. 3).

Electrophysiological properties of TRPC6 inhibition

As expected, ionic currents through mutant TRPC6 constructs resembled those of wild-type TRPC6 in terms of current-voltage-relationship, and their activation by 50 μM OAG (Fig. 4). With the exception of the E897K mutant, peak current densities were markedly higher than those seen in cells expressing the wild-type TRPC6. In all investigated channel constructs, the acute addition of 0.2 μM LC partially and 1 μM LC almost completely abolished the OAG-induced inward and outward currents measured at -100 mV and +100 mV, respectively. The block by 0.2 μM or 1 μM LC developed within a few seconds, which was sufficiently fast to qualitatively discern the channel inhibition from the slower channel inactivation, which was observed in cells that were not exposed to the inhibitor (see grey traces in Fig. 4B-H).

To obtain more detailed information about the inhibition of TRPC6 currents by LC in an equilibrium state of inhibitor binding, we exposed stably transfected HEK_{hTRPC6-YFP} cells to various concentrations of LC prior to stimulating channel activity with 50 μM OAG. In voltage ramp protocols applied in 1-s intervals, both inward currents measured at -100 mV and outward currents at +100 mV were concentration-dependently suppressed by LC (Fig. 5A-C). The corresponding IC_{50} values were 118 and 120 nM, respectively. Accordingly, currents measured during application of voltage ramps showed no signs of a voltage-dependent inhibition, and reversal potentials remained unchanged (Fig. 5B), indicating no major impact on the selectivity of conducted cations. In HEK293 cells expressing mutated TRPC6 constructs, preincubation with 1 μM LC for 1 min prior to OAG application significantly inhibited all tested TRPC6 variants (Fig. 5D). Since the inhibition amounted 70%-95%, we conclude that, like in wild-type TRPC6, the IC_{50} of LC to inhibit FSGS-related TRPC6 mutations is in a sub-micromolar concentration range.

Larixyl carbamate does not cause changes of the membrane potential and of TRPC6 expression

Since some pimarane compounds, which are chemically related to larixol, have been identified as modulators of large conductance Ca^{2+} -activated K^+ (BK) channels, we investigated whether LC can alter the membrane potential (E_m) in rat PASMC that endogenously express BK channels and voltage-dependent calcium channels (VDCC). Since the acute addition of 5 μM LC did not cause an increase in $[\text{Ca}^{2+}]_i$ in fura-2-loaded

PASMC (Fig. 6A), an efficient activation of VDCC could be excluded. In PASMC loaded with the E_m -sensitive fluorescent dye DiBAC₄(3), the direct TRPC6 activator GSK1702934A (10 μ M) caused a significant increase in DiBAC₄(3) fluorescence by $34.4\% \pm 17.3\%$ ($n = 8$), indicating a depolarisation. The known BK channel activator NS1619 (30 μ M) caused a decrease in DiBAC₄(3) fluorescence by $42.9\% \pm 11.4\%$ ($n = 7$), indicating a hyperpolarisation. By contrast, neither 5 μ M LMA nor 5 μ M LC caused a change in DiBAC₄(3) fluorescence compared to the solvent controls (Fig. 6B,C).

To analyse a possible impact of long-term incubation with LC on the global expression of TRPC6 in recombinantly and in natively TRPC6 expressing cells, Western blot analyses were performed in samples obtained from stably transfected HEK_{hTRPC6-YFP} cells and from rat PASMCs (three independent experiments, each) that were grown for 24 h in the presence of 5 and 10 μ M LC. The global abundance of heterologously expressed or of native TRPC6 remained largely unaffected by the TRPC6 inhibitor (Fig. 6D-F). Furthermore, since OAG-induced increases in $[Ca^{2+}]_i$ measured in PASMC after long-term (24 h) treatment with LC, followed by an acute wash-out of the inhibitor were not significantly different from those measured without preincubation of the TRPC6 inhibitor (see Fig. 6A), we conclude that the availability of TRPC6 channels at the cell surface is presumably not grossly affected by long term treatment with LC.

Isolation of glomeruli and of primary podocyte cultures

The isolation of mouse or rat glomeruli from the renal cortex usually involves a fractional sieving technique. Critical differences may rely on the way how glomeruli are being detached from surrounding tissue. Different options have been described: first a mechanical dissociation method by squeezing renal cortex through a mesh, and second an enzymatic digestion of minced pieces of renal cortex. In our hands, the latter one was suitable to obtain short-term cultures, which are highly enriched for podocytes. This observation was supported by the following evidence: (i) glomeruli fractions displayed a lower contamination with tubuli, (ii) Bowman's capsules were more efficiently removed, causing a strong increase in the relative abundance of podocin transcripts in quantitative RT-PCR and (iii) an efficient enrichment of podocin as seen in Western blot analyses (Fig. 7A,B). Finally, immunofluorescence staining of glomeruli with antibodies raised against the podocyte-specific marker podocin and the mesangial-specific marker α -SMA also confirmed the existence of podocytes and a well preserved structure of decapsulated rat or mouse glomeruli (Fig. 7C-E). By culturing them, we obtained podocin-positive podocyte cultures that

exhibited the typical cobblestoned and, later on, a beginning arborized morphology (Fig. 7F-H). A few mesangial cells also grew out of glomeruli, but they show a more elongated morphology and were positive for α -SMA staining (Fig. 7I-K).

Ca²⁺ signalling in isolated rat and mouse podocytes and glomeruli

In short-term cultures of enzymatically isolated rat and mouse podocytes, activation of P2Y, PAR1 or bradykinin receptors yielded the most robust [Ca²⁺]_i signals (Fig. 8A-E). As described earlier, functional expression of AT₁ receptors is rapidly lost in podocytes during the culturing. Accordingly, only in 2 out of 9 experiments, a fraction of rat podocytes (up to 35%) still responded to 10 μ M angiotensin II with a small Ca²⁺ mobilisation signal. In mouse podocytes, no increases in [Ca²⁺]_i were elicited by angiotensin II. During acute exposure to 100 μ M OAG, we did not observe a statistically significant increase in [Ca²⁺]_i in rat or mouse podocytes (see Fig. 8C-E). As expected, preincubation of mouse podocytes with thapsigargin induced a transient increase in [Ca²⁺]_i, but a subsequent challenge with 100 μ M ATP, 10 μ M bradykinin or 0.5 U/ml thrombin failed to cause a significant second increase in [Ca²⁺]_i (Supplemental Figure 1), which would be expected if cells were expressing substantial amounts of TRPC6. Likewise, the acute application of 5 μ M LMA did not cause rapid decline of the [Ca²⁺]_i in ATP-, bradykinin- or thrombin-stimulated mouse podocyte cultures (Fig. 8G) and even if 5 μ M LC was preincubated, the GPCR-induced [Ca²⁺]_i peaks did not diminish (Fig. 8F). The recently disclosed compound GSK1702934A is currently the most potent and effective direct activator of TRPC3 and TRPC6 channels. In multiwell calcium measurements, we obtained an EC₅₀ of 1.8 μ M for GSK1702934A to activate Ca²⁺ influx in stably transfected HEK_{hTRPC6-YFP} cells whereas the EC₅₀ of OAG and flufenamic acid (FFA) were 21.4 μ M and over 200 μ M (Supplemental Figure 2). Moreover, FFA seemed to provoke unspecific effects on parental HEK293 cells at high concentrations (see Supplemental Fig. 2A). Unfortunately, also 20 μ M GSK1702934A failed to elicit [Ca²⁺]_i signals in rat and mouse podocytes like demonstrated in PASMC from Wistar rats. By contrast, in PASMC prepared from the same animals, GSK1702934A induced a robust [Ca²⁺]_i signal (see Supplemental Fig. 2C-F), demonstrating that the compound indeed activates native TRPC6- and/or TRPC3-bearing channel complexes.

Since TRPC6 expression may be quickly down-regulated after the cell isolation, we also sought to observe TRPC6-related [Ca²⁺]_i signals in acutely dissociated mouse or rat glomeruli. Rat glomeruli robustly responded upon stimulation with 100 μ M carbachol (Fig. 9A). However, acute addition of 5 μ M LMA during the plateau phase of [Ca²⁺]_i elevation did

not significantly lower the $[Ca^{2+}]_i$ (Fig. 9B). Similar results were obtained with glomeruli isolated from transgenic B6.Cg-Tg(NPHS2-Trpc6) F419Walz/J mice (Fig. 9C,D). In glomeruli from these mice, pretreatment with 5 μ M LC also failed to exert a discernible impact on the size or on the kinetic properties of angiotensin II (10 μ M)-induced $[Ca^{2+}]_i$ signals (Fig. 9E-G). To exclude that our isolation procedure with collagenase may cause the lack of a discernible TRPC6 activation, we also used the mechanical squeezing method. Regardless of the isolation method, the TRPC6 activator GSK1702934A did not cause a discernible Ca^{2+} influx in any cell type of freshly isolated rat or mouse glomeruli. By contrast, stimulation with carbachol or with angiotensin II was still effective (see Supplemental Fig. 2E-F), indicating that small peptides and chemical compounds can access the cells. Increasing the driving force for calcium entry through TRPC6 by elevating the $CaCl_2$ concentration in the buffer from 1 mM to 2 mM had no effect. Since LMA-sensitive TRPC6-like responses were previously seen in short-term cultures of rat PASM (Urban *et al.*, 2016), which also responded to stimulation with the TRPC6 activator GSK1702934A (Supplemental Fig. 3C), the obvious question arose, how TRPC6 expression in podocytes compares to that in PASM.

TRPC6 expression in rat and mouse podocyte cultures and glomeruli compared to PASM

First, quantitative RT-PCR was applied to analyse the abundance of TRPC6-encoding transcripts in podocyte cultures obtained from rats, from wild-type mice or from transgenic mice, selectively overexpressing mouse TRPC6 in podocytes (under the control of a human podocin promoter/enhancer sequence). PCR products with the expected sizes for endogenously expressed rat or mouse TRPC6 were found in podocytes as well as in PASM isolated from several investigated animals (Fig. 10A,B). The selective detection of the transgene was positive in the TRPC6-overexpressing transgenic mouse strain, but not in wild-type mice (Fig. 10C). Quantitative PCR normalised to ribosomal 18s RNA revealed that in podocytes from 10 days-old or adult rats, TRPC6 mRNA was markedly less abundant than in rat PASM (Fig. 10D). Podocin expression was stronger in podocytes isolated from young animals, compared to podocytes from adult rats or to PASM, which also showed the highest relative expression of α -SMA (Fig. 10E). In podocytes isolated from wild-type mice, TRPC6 expression was again lower than in PASM isolated from the same animals. As expected, the mRNA abundance of mouse TRPC6 tended to be higher in podocytes from mice expressing the TRPC6 transgene than in age-matched wild-type mice, but was still

about 6-fold lower than endogenous TRPC6 expression in mouse PASMCM (Fig. 10F). The expression profile of podocin and α -SMA in wild-type or transgenic mice was similar to that observed in adult rats (see Fig. 10G).

At the protein level, demonstration of TRPC6 expression is limited by the quality of the antibodies. Western blot analyses clearly demonstrated TRPC6 expression in transiently transfected HEK293 cells, but two additional, unspecific bands were also seen in untransfected cells, or in control-transfected HEK293 cells expressing TRPC2-HA, TRPC3-HA or a soluble enhanced yellow fluorescent protein (Fig. 10H-J). Accepting the single specific band as an intraexperimental size marker for TRPC6, lysates of acutely dissociated rat or mouse glomeruli, podocyte or PASMCM cultures were judged. Specific signals were found in rat PASMCM cultures, but absent or markedly less intense in lysates from glomeruli (Fig. 10H,I) or podocyte cultures (Fig. 10J). Controls for the tissue and cell preparations were performed by probing the membranes with anti-podocin, and anti- α -SMA antibodies. In addition, a loading control was included (anti-GAPDH) in the experiments. From these data, we conclude that both mRNA and protein abundance of TRPC6 are highly dissimilar between PASMCM and podocytes or glomeruli. Thus, the lack of TRPC6-like global $[Ca^{2+}]_i$ signals may be explained by the limited sensitivity of fluorometric analyses under conditions of low channel expression, which was not overcome by the moderate, podocyte-specific TRPC6 overexpression in a transgenic B6.Cg-Tg(NPHS2-Trpc6)F419Walz/J mouse line.

Ionic currents in rat and mouse podocytes

In electrophysiological recordings, the sensitivity of detecting minute TRPC6 currents may be higher than in fluorometric $[Ca^{2+}]_i$ analyses. We therefore attempted to assess the sensitivity of native TRPC6 to inhibition by LMA and LC by measuring whole-cell currents in primary cultures of mouse and rat podocytes. Applying a voltage ramp protocol, an increase in ionic currents could be elicited by stimulation with OAG in 10 out of 34 patched rat podocytes. Figure 9A depicts current densities in one of these cells, more examples are shown in Supplementary Figure 1. The reversal potential was close to 0 mV, indicating a non-selective conductance. Leak-subtracted increases in current densities upon stimulation with 50 μ M OAG were 0.648 ± 0.126 pA/pF and 1.267 ± 0.359 pA/pF, measured at -100 mV and + 100 mV, respectively. In these podocytes, the acute addition of 5 μ M LMA (see Supplementary Fig. 1A) or of 2.5 μ M LC (Fig. 11A and Supplementary Fig. 3B-D) caused a rapid decline of inward currents at -100 mV by 1.069 ± 0.321 pA/pF, and of outward currents at +100 mV of 2.161 ± 0.746 pA/pF at +100 mV. The LMA- or LC-sensitive current

components again displayed a reversal potential close to 0 mV and outwardly rectifying properties, which is compatible with TRPC6 being the modulated channel entity.

In podocytes cultures obtained from TRPC6-overexpressing transgenic mice, similar results were obtained (Fig. 11B and Supplementary Fig. 3E-H). Here, OAG induced increases in current densities in 20 out of 45 patched cells. Current density increases over basal currents amounted 0.563 ± 0.162 pA/pF at -100 mV, and 1.126 ± 0.213 pA/pF at +100 mV. The acute addition of LMA or LC caused decreases in inward and outward current densities by 0.717 ± 0.173 pA/pF and 1.753 ± 0.412 pA/pF, measured at -100 mV and +100 mV, respectively. Like in rat podocytes, all mouse podocytes that displayed a discernible increase in current densities when challenged with OAG also responded to the addition of LMA or LC with a current inhibition. From these data we conclude that TRPC6-like conductances in primary rodent podocyte cultures are small, but sensitive to the semisynthetic larixol derivatives. For comparison, the OAG-activated non-selective ion current densities measured under the same conditions in rat PASMCM were -2.46 ± 0.93 and 21.27 ± 5.23 pA/pF at -100 mV and +100 mV, respectively (data not shown).

4. Discussion

Within canonical TRPC channels, gain of function mutations of TRPC6 in familiar forms of FSGS represent the best characterised channelopathy, which leads to an as yet untreatable focal segmental glomerulosclerosis, culminating in end-stage kidney disease. Adding to this still unmet medical need, lung diseases, such as pulmonary hypertension, allergic airway hyperresponsiveness, and ischemia/reperfusion-induced lung oedema, are potential fields of application for inhibitory pharmacological modulators of TRPC6 activity (Bon & Beech, 2013; Mene *et al.*, 2013). We here propose larixyl carbamate as a semisynthetic larixol derivative, which is easily available, highly efficient and potent in suppressing TRPC6-mediated Ca^{2+} influx and ionic currents in both heterologous expression systems as well as in native cell models of TRPC6 activity. The biological activity of LC was reassessed and approved in various mutated TRPC6 constructs, carrying FSGS-related nonsynonymous substitutions. During the process of validating the blocker efficiency in native cells, we faced the problem that native TRPC6-like responses were hardly detectable in primary podocyte cultures or in freshly isolated glomeruli from rats or mice, including a transgenic mouse strain, which moderately overexpresses TRPC6 under the control of a podocyte-specific promoter (Krall *et al.*, 2010). To elucidate the apparent discrepancy, we assessed the mRNA

and protein abundance in podocytes and glomeruli compared to pulmonary artery smooth muscle cells. The about 20- to 50-fold lower abundance of TRPC6 mRNA in podocytes and glomeruli provided an explanation for the lack of strong TRPC6-like signals in fluorometric $[Ca^{2+}]_i$ assays. In electrophysiological patch clamp experiments, the expected low current densities were seen, and the efficiency of larixyl carbamate to inhibit these currents could be demonstrated. Thus, despite its weak expression, up-regulated wild-type TRPC6 or mutated TRPC6 variants seem to play seminal roles in causing podocyte injury in diseased states. We expect that more selective and validated TRPC6 inhibitors will be instrumental to explore the therapeutic potential of pharmacological interference with this target.

Our development of new TRPC6 inhibitors originated from larixyl monoacetate (Urban *et al.*, 2016), and revealed larixyl carbamate as a highly potent derivative, which is biologically active with respect to native TRPC6 as well as to six human TRPC6 variants carrying mutations known to cause FSGS. In comparison to some other TRPC6 inhibitors like norgestimate (Miehe *et al.*, 2012) or compound 8009-5364 (Urban *et al.*, 2012), the selectivity of LMA or LC to inhibit TRPC6 but not their closest related channels TRPC3 and TRPC7 is considerably higher. The highly potent TRPC6 inhibitor (Maier *et al.*, 2015) displays an even higher potency and selectivity than LC, but its efficiency and potency to inhibit FSGS-related TRPC6 mutations has not been confirmed so far. Experiments with single cell $[Ca^{2+}]_i$ measurements and electrophysiological trials demonstrated that high nanomolar or low micromolar concentrations of either LMA or LC are sufficient to inhibit the activity of FSGS-related TRPC6 channel constructs to levels of wild-type TRPC6 or below. Since TRPC6-associated FSGS is an autosomal dominant disease in which a wild-type allele coexists, and since mutations are located in intracellular domains that may affect the channel assembly, we explored if mutated TRPC6 channels still maintain their ability to form channel complexes together with the wildtype subunits. FRET analyses clearly demonstrated that the investigated point mutations do not grossly affect the oligomerisation properties of the channel. Thus, although some mutated TRPC6 variants seemed to require slightly higher LMA or LC concentrations for half-maximal inhibition, a heteromeric complex formed by the gene products of the mutated and wild-type alleles may further reduce these differences. Sub-micromolar IC_{50} values provide a promising starting point for a more detailed investigation in preclinical disease models examinations and experimental therapies that critically involve TRPC6 activity. Featuring a carbamyl group rather than an ester-bonded acetate, LC may resist intracellular esterases. Of note, the pharmacophore of LC is chemically unrelated to that of SAR7334. Thus, observing similar effects with both inhibitors

would strengthen the evidence for an involvement of TRPC6 in biological activities that are modulated by either drug.

A medical need for TRPC6 inhibitors is best exemplified by hereditary forms of FSGS that involve gain of function mutations in TRPC6. We therefore aimed at characterising six of the previously described TRPC6 mutations that have been reported to cause hyperactive channel complexes (Reiser *et al.*, 2005; Winn *et al.*, 2005; Heeringa *et al.*, 2009; Hofstra *et al.*, 2013; Zhu *et al.*, 2009). Our findings confirmed the phenotype of the P112Q-, M132T-, R175Q- and Q889K-variants that displayed significantly higher basal activity and OAG-induced peaks in single-cell $[Ca^{2+}]_i$ measurements, and larger current densities in electrophysiological patch-clamp experiments. Interestingly, the apparent activity of the R895C variant showed a discrepancy between applied experimental methods. Basal $[Ca^{2+}]_i$ and the OAG-induced peak currents in electrophysiological experiments were significantly increased compared to wild-type TRPC6, which is compatible with previous reports (Reiser *et al.*, 2005; Schlöndorff *et al.*, 2009; Hofstra *et al.*, 2013). However, we did not observe significantly elevated $[Ca^{2+}]_i$ values after OAG addition in single cell $[Ca^{2+}]_i$ measurements. In our experiments, the E897K mutation displayed no significant hyperactivity in either method. In carbachol-stimulated HEK293-M1 cells that stably express the M1 muscarinic receptor, Reiser *et al.* reported higher current densities for E897K-mutated TRPC6 (15924139). Applying the same construct, Schlöndorff *et al.* have described a trend to lower basal current amplitudes, and an elevated basal $[Ca^{2+}]_i$ was only seen in a subset of HEK293-M1 cells that express the R895C or E897K variants (Schlöndorff *et al.*, 2009). It is known that the receptor-activated signals are significantly larger than those after direct TRPC6 activation with the membrane-permeable DAG mimic OAG (Estacion *et al.*, 2004). Hence, the different modes of TRPC6 activation and differences in the cellular background may explain the differences. Since LC efficiently inhibits Ca^{2+} entry and ionic currents through the E897K-mutated TRPC6, its use would still be justified e.g. in a preclinical disease model given by a transgenic mouse strain that overexpress the E897K variant and develops FSGS-like glomerular lesions (Krall *et al.*, 2010).

In podocytes, TRPC6 is the predominant Ca^{2+} -permeable channel that promotes stress fibre formation via RhoA activity and thereby mediates the contractile phenotype in these cells (Tian *et al.*, 2010). Furthermore, TRPC5 has been implicated to be involved in podocyte migration by increasing Rac1 activation and a loss of stress fibres (Tian *et al.*, 2010; Schaldecker *et al.*, 2013). Under physiological conditions, both TRPC6 and TRPC5 are activated by angiotensin II downstream of the AT_1 receptor (Tian *et al.*, 2010; Eckel *et al.*,

2011), whereupon DAG generated from phosphatidylinositol-4,5-bisphosphate by PLC directly and activates TRPC6 (Hofmann *et al.*, 1999; Sonneveld *et al.*, 2014). Performing microfluorometric $[Ca^{2+}]_i$ imaging experiments with podocytes, we therefore initially aimed at activating endogenous TRPC6 channels with the membrane-permeable DAG analog OAG. Surprisingly, we could not detect a significant increase in $[Ca^{2+}]_i$ in primary podocyte cultures from rat and mice. Applying angiotensin II instead of OAG, we found that the $[Ca^{2+}]_i$ signals were inconsistent and not significantly impaired by preincubation with LMA or LC. To activate other GPCRs that are known to be expressed in podocytes (Nitschke *et al.*, 2001; Madhusudhan *et al.*, 2012; Ilatovskaya *et al.*, 2013; Roshanravan & Dryer, 2014), we also tested ATP, bradykinin, carbachol or thrombin as activators, but TRPC6-like activities remained undetectable in microfluorometric $[Ca^{2+}]_i$ analyses. It is known that podocytes rapidly de-differentiate under cell culture conditions. This process is characterised by a loss of foot processes and of podocyte-specific proteins, such as synaptopodin, podocin or the AT_1 receptor (Shankland *et al.*, 2007). Hence, a small and inconsistent $[Ca^{2+}]_i$ signal upon addition of angiotensin II was not unexpected. Other groups have faced the same problem and, to circumvent it, sometimes re-introduced the AT_1 receptor by transient transfection (Tian *et al.*, 2010). The lack of a discernible TRPC6 activation by OAG nonetheless intrigued us, because endogenously expressed TRPC6 is functionally detectable in freshly isolated PSMCs (Weissmann *et al.*, 2006; Fuchs *et al.*, 2011; Urban *et al.*, 2016). We also obtained the transgenic mouse strain which overexpresses TRPC6 in podocytes and develops an FSGS-like phenotype (Krall *et al.*, 2010). Nevertheless, a TRPC6-like Ca^{2+} influx was also not detectable in isolated podocytes from this mouse strain, applying OAG in fluorometric assays. In line with the author's description of a 2-fold elevation of TRPC6 mRNA levels in glomeruli from this mouse, and of low abundance of the TRPC6 protein (Krall *et al.*, 2010), a mild podocyte-specific increase in TRPC6 expression may still not suffice to augment TRPC6-like Ca^{2+} influx signal above detection thresholds. Of note, all studies that demonstrate a robust OAG-mediated Ca^{2+} influx in podocyte cultures used immortalised mouse or human podocyte cell lines rather than primary cultures (Möller *et al.*, 2007; Nijenhuis *et al.*, 2011; Yang *et al.*, 2013; Sonneveld *et al.*, 2014; Ambrus *et al.*, 2015). Cultured podocytes lose their cell microarchitecture, receptors or ion channels *in vitro*. We therefore next focused on freshly isolated intact glomeruli. Here, carbachol- and angiotensin II-induced increases in $[Ca^{2+}]_i$ have been reported for rat and mouse glomeruli (Nitschke *et al.*, 2000; Nitschke *et al.*, 2001). Our data are in good agreement with these findings. However, the recently published inhibition of angiotensin II-induced $[Ca^{2+}]_i$ signals by SKF-

96365 (Ilatovskaya *et al.*, 2014) was not reproducible with the TRPC6 inhibitors LMA or LC. In our hands, 1 μM SKF-96365 is not sufficiently effective to block recombinant TRPC6, and single channel properties of TRPC6 are characterised by markedly shorter open times, very low spontaneous activity, an almost instantaneous opening after GPCR stimulation, a more rapid deactivation, a voltage-dependence of their open probability, and a larger unitary conductance (Hofmann *et al.*, 1999, Urban *et al.* 2016). In rat glomeruli, the more long-lasting carbachol-induced $[\text{Ca}^{2+}]_i$ signal enabled an acute application of LMA, but again the signal did not seem to critically depend on TRPC6. Finally, our analyses of TRPC6 mRNA and protein in freshly isolated glomeruli and in cultured podocytes provided an explanation for the absence of robust TRPC6-related $[\text{Ca}^{2+}]_i$ signals. The about 20 to 50-fold lower abundance of TRPC6 mRNA in podocytes compared to PASMCs matched with electrophysiological findings. OAG-induced current densities in PASMCs were about 20-fold higher than in podocytes, which only reached about 1 pA/pF. Interestingly, few studies utilizing freshly isolated podocytes instead of the immortalized cell lines confirmed these very small current amplitudes upon stimulation with angiotensin II (Eckel *et al.*, 2011; Kalwa *et al.*, 2015).

The partial inhibition of TRPC6 activity by low concentrations LMA or LC may be exploited to design experimental therapies in pulmonary and renal diseases. For example, about 0.5-2 μM LC suppressed ionic currents through the most strongly overactive TRPC6 mutations (P112Q, M132T, and R175Q) to a level that corresponds to those of wild-type TRPC6. In pulmonary diseases or to prevent ischemia-reperfusion-induced pulmonary oedema e.g. in a scenario of lung or combined heart-lung transplantation, a beneficial effect of TRPC6 inhibition still needs to be demonstrated. Consequently, the required systemic plasma concentrations or tissue concentrations of TRPC6 inhibitors are not yet established. In the lung or in organ transplantation, however, topical application or addition to the preservation fluid may limit systemic effects of TRPC6 inhibitors and thereby increase the tolerability and safety of use. In familial forms of FSGS, a lifelong application of TRPC6 inhibitors e.g. in carriers of TRPC6 mutations may be considered to prevent or at least delay the onset of nephrotic syndrome and requirement of kidney transplantation. On the other hand, since TRPC6 may also exert protective functions in complement-dependent forms of glomerular injury (Kistler *et al.*, 2013), the risk to benefit ratio of pharmacological TRPC6 inhibition needs to be critically evaluated. Appropriate animal models of human kidney or lung diseases together with validated new TRPC6 inhibitors, such as LC or aminoindanes (Maier *et al.*, 2015) now provide a rational basis for the validation of TRPC6 as a pharmacological

target by designing preclinical models, assessment of the safety profile, and by testing their efficacy and tolerability in experimental therapies.

Conflict of interest

The authors declare no conflicts of interest.

Acknowledgments

We thank Anne-Kathrin Krause for expert technical assistance and animal care and Thomas Rudolph for technical support of the chemical synthesis and analysis. This work was supported by the Deutsche Forschungsgemeinschaft (TRR 152 to M.S. and TRR 67 to J.R.).

Accepted Article

References

- Abkhezr, M, Kim, EY, Roshanravan, H, Nikolos, F, Thomas, C, Hagmann, H, et al. (2015). Pleiotropic signaling evoked by tumor necrosis factor in podocytes. *Am J Physiol Renal Physiol*, **309**, F98-108.
- Abramoff, MD & Magalhaes, PJ. (2004). Image processing with ImageJ. *Biophotonics International*, **11**, 36-42.
- Ambrus, L, Olah, A, Olah, T, Balla, G, Saleem, MA, Orosz, P, et al. (2015). Inhibition of TRPC6 by protein kinase C isoforms in cultured human podocytes. *J Cell Mol Med*, **19**, 2771-2779.
- Anderson, M, Roshanravan, H, Khine, J & Dryer, SE. (2014). Angiotensin II activation of TRPC6 channels in rat podocytes requires generation of reactive oxygen species. *J Cell Physiol*, **229**, 434-442.
- Bon, RS & Beech, DJ. (2013). In pursuit of small molecule chemistry for calcium-permeable non-selective TRPC channels - mirage or pot of gold? *Br J Pharmacol*, **170**, 459-474.
- Dietrich, A & Gudermann, T. (2014). TRPC6: physiological function and pathophysiological relevance. *Handb Exp Pharmacol*, **222**, 157-188.
- Eckel, J, Lavin, PJ, Finch, EA, Mukerji, N, Burch, J, Gbadegesin, R, et al. (2011). TRPC6 enhances angiotensin II-induced albuminuria. *J Am Soc Nephrol*, **22**, 526-535.
- Edelstein, A, Amodaj, N, Hoover, K, Vale, R & Stuurman, N. (2010). Computer control of microscopes using microManager. *Curr Protoc Mol Biol*, **Chapter 14**, Unit14.
- Ei, HS & Reiser, J. (2011). TRPC channel modulation in podocytes-inching toward novel treatments for glomerular disease. *Pediatr Nephrol*, **26**, 1057-1064.
- Estacion, M, Li, S, Sinkins, WG, Gosling, M, Bahra, P, Poll, C, et al. (2004). Activation of human TRPC6 channels by receptor stimulation. *J Biol Chem*, **279**, 22047-22056.
- Fuchs, B, Rupp, M, Ghofrani, HA, Schermuly, RT, Seeger, W, Grimminger, F, et al.. (2011). Diacylglycerol regulates acute hypoxic pulmonary vasoconstriction via TRPC6. *Respir Res*, **12**, 20.
- Gigante, M, Caridi, G, Montemurno, E, Soccio, M, d'Apolito, M, Cerullo, G, et al. (2011). TRPC6 mutations in children with steroid-resistant nephrotic syndrome and atypical phenotype. *Clin J Am Soc Nephrol*, **6**, 1626-1634.
- Heeringa, SF, Moller, CC, Du, J, Yue, L, Hinkes, B, Chernin, G, et al. (2009). A novel TRPC6 mutation that causes childhood FSGS. *PLoS One*, **4**, e7771.
- Hellwig, N, Albrecht, N, Harteneck, C, Schultz, G & Schaefer, M. (2005). Homo- and heteromeric assembly of TRPV channel subunits. *J Cell Sci*, **118**, 917-928.
- Hofmann, T, Obukhov, AG, Schaefer, M, Harteneck, C, Gudermann, T & Schultz, G. (1999). Direct activation of human TRPC6 and TRPC3 channels by diacylglycerol. *Nature*, **397**, 259-263.

- Hofmann, T, Schaefer, M, Schultz, G & Gudermann, T. (2002). Subunit composition of mammalian transient receptor potential channels in living cells. *Proc Natl Acad Sci U S A*, **99**, 7461-7466.
- Hofstra, JM, Lainez, S, van Kuijk, WH, Schoots, J, Baltissen, MP, Hoefsloot, LH, et al. (2013). New TRPC6 gain-of-function mutation in a non-consanguineous Dutch family with late-onset focal segmental glomerulosclerosis. *Nephrol Dial Transplant*, **28**, 1830-1838.
- Ilatovskaya, DV, Palygin, O, Chubinskiy-Nadezhdin, V, Negulyaev, YA, Ma, R, Birnbaumer, L, et al. (2014). Angiotensin II has acute effects on TRPC6 channels in podocytes of freshly isolated glomeruli. *Kidney Int*, **86**, 506-514.
- Ilatovskaya, DV, Palygin, O, Levchenko, V & Staruschenko, A. (2013). Pharmacological characterization of the P2 receptors profile in the podocytes of the freshly isolated rat glomeruli. *Am J Physiol Cell Physiol*, **305**, C1050-C1059.
- Ilatovskaya, DV & Staruschenko, A. (2015). TRPC6 channel as an emerging determinant of the podocyte injury susceptibility in kidney diseases. *Am J Physiol Renal Physiol*, **309**, F393-F397.
- Kalwa, H, Storch, U, Demleitner, J, Fiedler, S, Mayer, T, Kannler, M, et al. (2015). Phospholipase C ϵ induced TRPC6 activation: a common but redundant mechanism in primary podocytes. *J Cell Physiol*, **230**, 1389-1399.
- Kim, EY, Anderson, M & Dryer, SE. (2012). Insulin increases surface expression of TRPC6 channels in podocytes: role of NADPH oxidases and reactive oxygen species. *Am J Physiol Renal Physiol*, **302**, F298-F307.
- Kistler, AD, Singh, G, Altintas, MM, Yu, H, Fernandez, IC, Gu, C, et al. (2013). Transient receptor potential channel 6 (TRPC6) protects podocytes during complement-mediated glomerular disease. *J Biol Chem*, **288**, 36598-36609.
- Krall, P, Canales, CP, Kairath, P, Carmona-Mora, P, Molina, J, Carpio, JD, et al. (2010). Podocyte-specific overexpression of wild type or mutant *trpc6* in mice is sufficient to cause glomerular disease. *PLoS One*, **5**, e12859.
- Lenz, JC, Reusch, HP, Albrecht, N, Schultz, G & Schaefer, M. (2002). Ca²⁺-controlled competitive diacylglycerol binding of protein kinase C isoenzymes in living cells. *J Cell Biol*, **159**, 291-302.
- Madhusudhan, T, Wang, H, Straub, BK, Grone, E, Zhou, Q, Shahzad, K, et al. (2012). Cytoprotective signaling by activated protein C requires protease-activated receptor-3 in podocytes. *Blood*, **119**, 874-883.
- Maier, T, Follmann, M, Hessler, G, Kleemann, HW, Hachtel, S, Fuchs, B, et al. (2015). Discovery and pharmacological characterization of a novel potent inhibitor of diacylglycerol-sensitive TRPC cation channels. *Br J Pharmacol*, **172**, 3650-3660.
- Mene, P, Punzo, G & Pirozzi, N. (2013). TRP channels as therapeutic targets in kidney disease and hypertension. *Curr Top Med Chem*, **13**, 386-397.
- Miehe, S, Crause, P, Schmidt, T, Lohn, M, Kleemann, HW, Licher, T, et al. (2012). Inhibition of diacylglycerol-sensitive TRPC channels by synthetic and natural steroids. *PLoS One*, **7**, e35393.

- Möller, CC, Wei, C, Altintas, MM, Li, J, Greka, A, Ohse, T, et al. (2007). Induction of TRPC6 channel in acquired forms of proteinuric kidney disease. *J Am Soc Nephrol*, **18**, 29-36.
- Nijenhuis, T, Sloan, AJ, Hoenderop, JG, Flesche, J, van Goor, H, Kistler, AD, et al. (2011). Angiotensin II contributes to podocyte injury by increasing TRPC6 expression via an NFAT-mediated positive feedback signaling pathway. *Am J Pathol*, **179**, 1719-1732.
- Nitschke, R, Henger, A, Ricken, S, Gloy, J, Müller, V, Greger, R et al. (2000). Angiotensin II increases the intracellular calcium activity in podocytes of the intact glomerulus. *Kidney Int*, **57**, 41-49.
- Nitschke, R, Henger, A, Ricken, S, Müller, V, Köttgen, M, Bek, M, et al. (2001). Acetylcholine increases the free intracellular calcium concentration in podocytes in intact rat glomeruli via muscarinic M₅ receptors. *J Am Soc Nephrol*, **12**, 678-687.
- Reiser, J, Polu, KR, Möller, CC, Kenlan, P, Altintas, MM, Wei, C, et al. (2005). TRPC6 is a glomerular slit diaphragm-associated channel required for normal renal function. *Nat Genet*, **37**, 739-744.
- Riehle, M, Büscher, AK, Gohlke, BO, Kassmann, M, Kolatsi-Joannou, M, Bräsen, et al. (2016). TRPC6 G757D loss-of-function mutation associates with FSGS. *J Am Soc Nephrol*, **27**, 2771-2783.
- Roshanravan, H & Dryer, SE. (2014). ATP acting through P2Y receptors causes activation of podocyte TRPC6 channels: role of podocin and reactive oxygen species. *Am J Physiol Renal Physiol*, **306**, F1088-F1097.
- Schaldecker, T, Kim, S, Tarabanis, C, Tian, D, Hakrrouch, S, Castonguay, P, et al. (2013). Inhibition of the TRPC5 ion channel protects the kidney filter. *J Clin Invest*, **123**, 5298-5309.
- Schlöndorff, J, Del, CD, Carrasquillo, R, Lacey, V & Pollak, MR. (2009). TRPC6 mutations associated with focal segmental glomerulosclerosis cause constitutive activation of NFAT-dependent transcription. *Am J Physiol Cell Physiol*, **296**, C558-C569.
- Shankland, SJ, Pippin, JW, Reiser, J & Mundel, P. (2007). Podocytes in culture: past, present, and future. *Kidney Int*, **72**, 26-36.
- Sonneveld, R, van der Vlag, J, Baltissen, MP, Verkaart, SA, Wetzels, JF, Berden, JH, et al. (2014). Glucose specifically regulates TRPC6 expression in the podocyte in an AngII-dependent manner. *Am J Pathol*, **184**, 1715-1726.
- Southan, C, Sharman, JL, Benson, HE, Faccenda, E, Pawson, AJ, Alexander, SP, et al. (2016). The IUPHAR/BPS Guide to PHARMACOLOGY in 2016: towards curated quantitative interactions between 1300 protein targets and 6000 ligands. *Nucl Acids Res*, **44**, D1054-1068.
- Sprangers, B, Meijers, B & Appel, G. (2016). FSGS: Diagnosis and Diagnostic Work-Up. *Biomed Res Int*, **2016**, 4632768.
- Szabo, T, Ambrus, L, Zakany, N, Balla, G & Biro, T. (2015). Regulation of TRPC6 ion channels in podocytes - Implications for focal segmental glomerulosclerosis and acquired forms of proteinuric diseases. *Acta Physiol Hung*, **102**, 241-251.

- Tian, D, Jacobo, SM, Billing, D, Rozkalne, A, Gage, SD, Anagnostou, T, et al. (2010). Antagonistic regulation of actin dynamics and cell motility by TRPC5 and TRPC6 channels. *Sci Signal*, **3**, ra77.
- Urban, N, Hill, K, Wang, L, Kuebler, WM & Schaefer, M. (2012). Novel pharmacological TRPC inhibitors block hypoxia-induced vasoconstriction. *Cell Calcium*, **51**, 194-206.
- Urban, N, Wang, L, Kwiek, S, Rademann, J, Kuebler, WM & Schaefer, M. (2016). Identification and validation of larixyl acetate as a potent TRPC6 inhibitor. *Mol Pharmacol*, **89**, 197-213.
- Wang, Z, Wei, X, Zhang, Y, Ma, X, Li, B, Zhang, S, et al. (2009). NADPH oxidase-derived ROS contributes to upregulation of TRPC6 expression in puromycin aminonucleoside-induced podocyte injury. *Cell Physiol Biochem*, **24**, 619-626.
- Weissmann, N, Dietrich, A, Fuchs, B, Kalwa, H, Ay, M, Dumitrascu, R, et al. (2006). Classical transient receptor potential channel 6 (TRPC6) is essential for hypoxic pulmonary vasoconstriction and alveolar gas exchange. *Proc Natl Acad Sci U S A*, **103**, 19093-19098.
- Winn, MP, Conlon, PJ, Lynn, KL, Farrington, MK, Creazzo, T, Hawkins, AF, et al. (2005). A mutation in the TRPC6 cation channel causes familial focal segmental glomerulosclerosis. *Science*, **308**, 1801-1804.
- Yang, H, Zhao, B, Liao, C, Zhang, R, Meng, K, Xu, J, et al. (2013). High glucose-induced apoptosis in cultured podocytes involves TRPC6-dependent calcium entry via the RhoA/ROCK pathway. *Biochem Biophys Res Commun*, **434**, 394-400.
- Zhu, B, Chen, N, Wang, ZH, Pan, XX, Ren, H, Zhang, W, et al. WM. (2009). Identification and functional analysis of a novel TRPC6 mutation associated with late onset familial focal segmental glomerulosclerosis in Chinese patients. *Mutat Res*, **664**, 84-90.

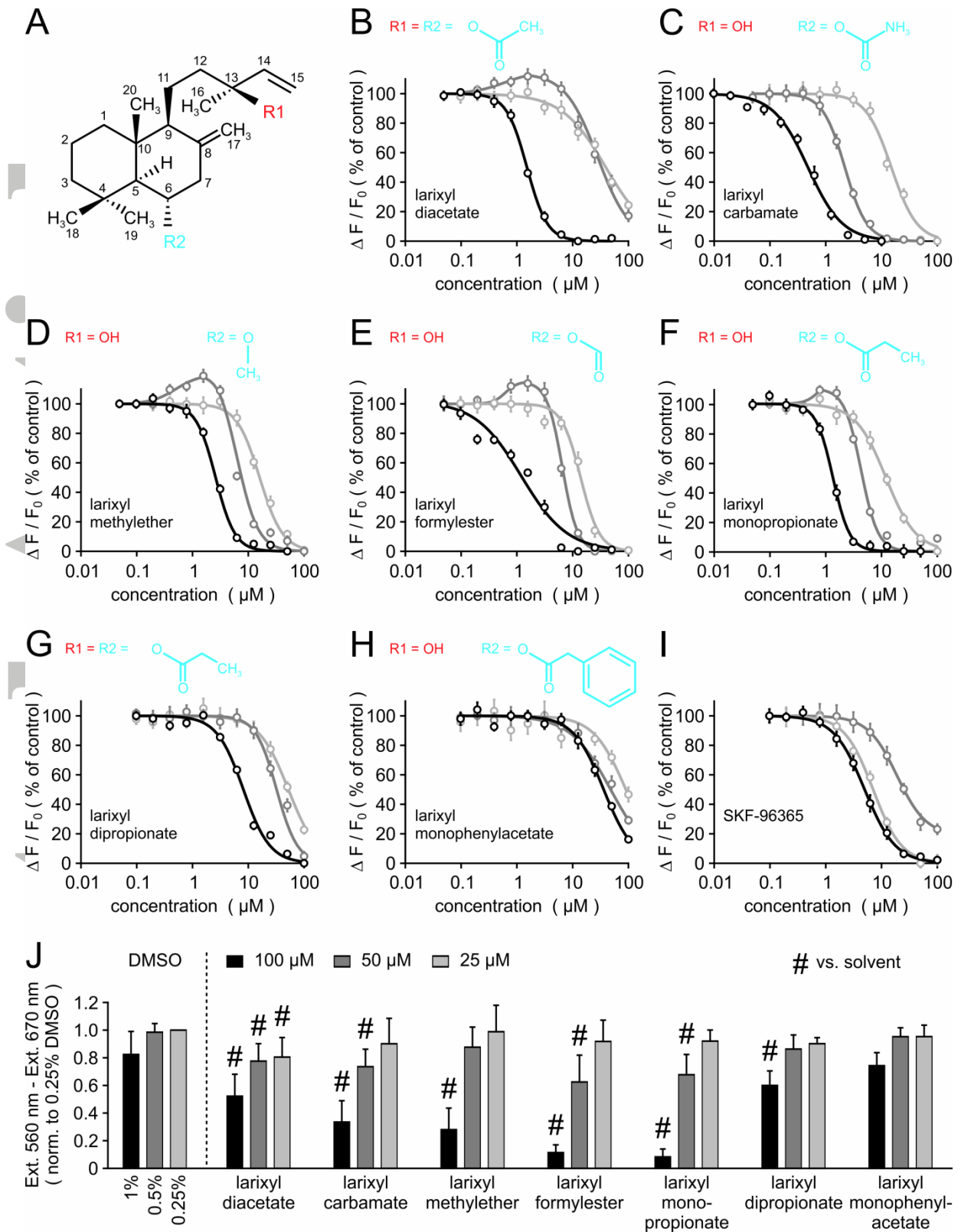


Figure 1: Semisynthetic larixol derivatives: potency and selectivity of to inhibit TRPC3, TRPC6, and TRPC7, and cytotoxicity.

Stably transfected HEK293 cell lines overexpressing TRPC3 (light grey lines), TRPC6 (black lines), or TRPC7 (dark grey lines) were loaded with the Ca^{2+} indicator dye fluo-4/AM,

washed, exposed to various serially diluted modulators, and assayed during stimulation with 50 μ M OAG in a fluorescence imaging plate reader device. (A) Chemical structure of the diterpene moiety of larixol with locant numbers and positions of the secondary and tertiary alcohols indicated as R1 and R2, respectively. (B-H) Concentration-response curves of OAG-induced Ca^{2+} signals detected in the presence of the indicated concentrations of the differently substituted larixyl compounds. Substituents at positions R1 and R2 are indicated. (I) Experiments performed as in (B-H), but with serially diluted SKF-96365 as poorly selective TRP channel modulator. Fluorescence intensity increases ΔF were normalised to the respective initial fluorescence intensity F_0 , and expressed as percentage of responses that were elicited in the absence of the compound. Data represent means and S.E. of 16-24 recordings obtained in 4-6 independent experiments. (J) Detection of HEK293 cell viability after 24 hour-treatment with larixol derivatives by using MTT assay. Bar graph shows means and SD of 6-8 experiments. #: significant changes compared to 0.25% DMSO controls (ANOVA with Dunn-Sidak test to correct for multiple comparisons).

Accepted Article

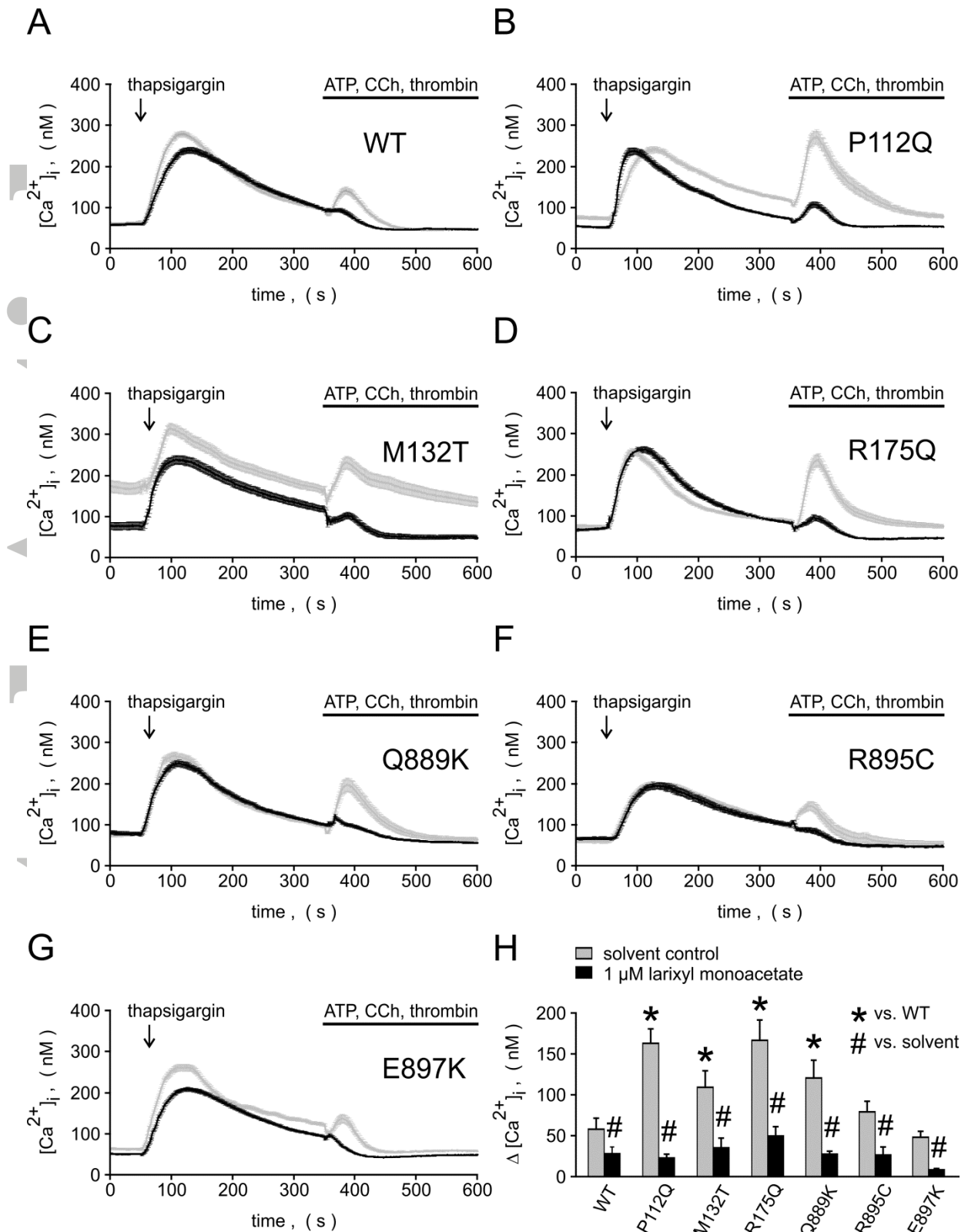


Figure 2: Fluorometric $[Ca^{2+}]_i$ analysis in HEK293 cells expressing wild-type or FSGS-related mutated TRPC6

Accepted Article

Adherent HEK293 cells were grown on glass coverslips and transiently transfected with expression plasmids encoding wild-type (WT; A) or the indicated point-mutated TRPC6 variants (B-G). After loading of the $[Ca^{2+}]_i$ indicator dye fura-2/AM, coverslips were subjected to microfluorometric single cell $[Ca^{2+}]_i$ analysis. Excitation wavelengths of 340 nm, 358 nm and 380 nm were sequentially applied and fluorescence emission was recorded at 500-550 nm with a cooled CCD camera. Cells were either kept in a bath solution containing 1 μ M LMA (black traces) or no TRPC6 inhibitor (grey lines). To deplete inositol-1,4,5-trisphosphate-sensitive storage organelles, 2 μ M thapsigargin was applied for 300 s before challenging cells with an activator mix, consisting of ATP (300 μ M), carbachol (CCH; 1 mM), and thrombin (0.5 units/ml). Note the elevated basal $[Ca^{2+}]_i$ in cells expressing the M132T mutant, which was counteracted by 1 μ M LMA. Shown are means and S.E. of 50-140 cells measured in a representative experiment. (H) Statistical analysis (means and S.E.) of 6 independent experiments each, performed as shown in (B-G). Significant changes were accepted at $p < 0.05$.

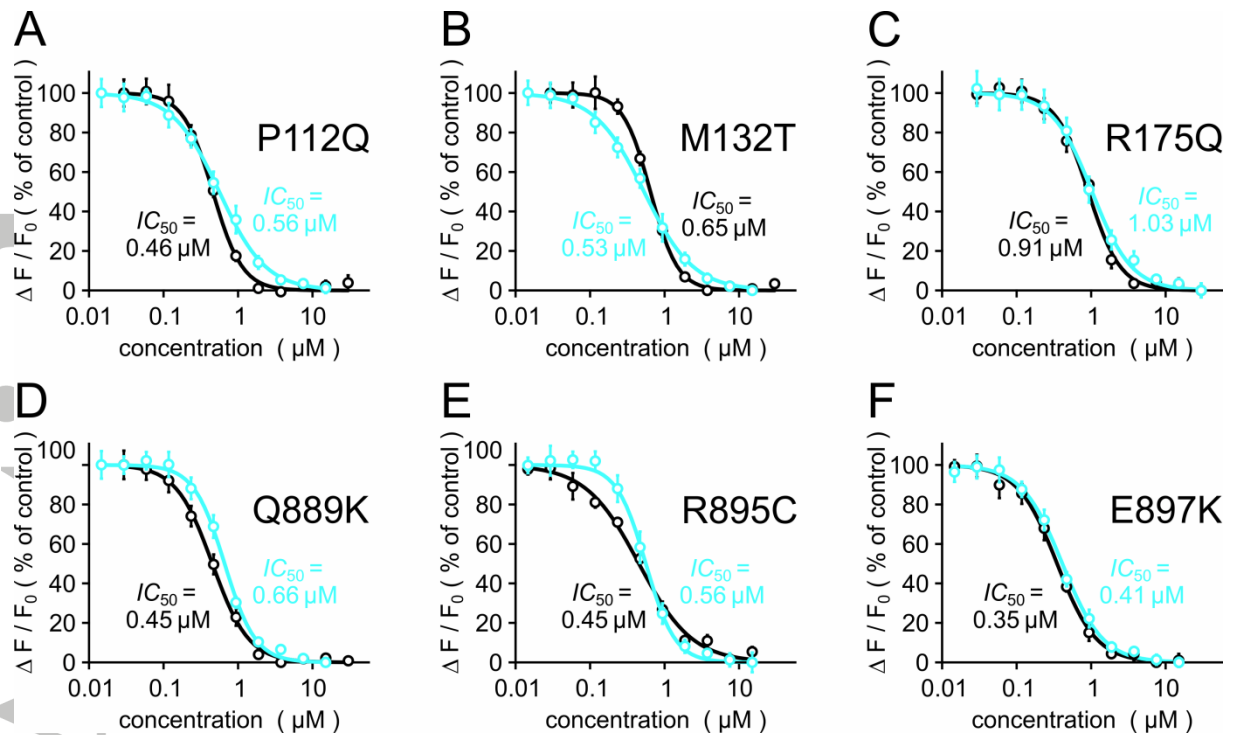


Figure 3: Concentration-dependent inhibition of Ca^{2+} influx through FSGS-related TRPC6 mutants by LMA and LC

Experiments were performed essentially as described in Figure 1, but with fluo-4-loaded stably transfected HEK293 cell lines, expressing the indicated point-mutated TRPC6 constructs. Fluo-4-loaded cell suspensions were incubated for 5 min with the indicated concentrations of LMA (black symbols and lines) or LC (blue) before activating TRPC6 with 50 μM OAG. Concentration response curves of the inhibition of OAG-induced Ca^{2+} signals were constructed by fitting four-parameter Hill equations to the experimental data. The resulting IC_{50} values are indicated. Data represent IC_{50} means and S.E. of 10-13 datasets, each, obtained in 4-7 independent experiments.

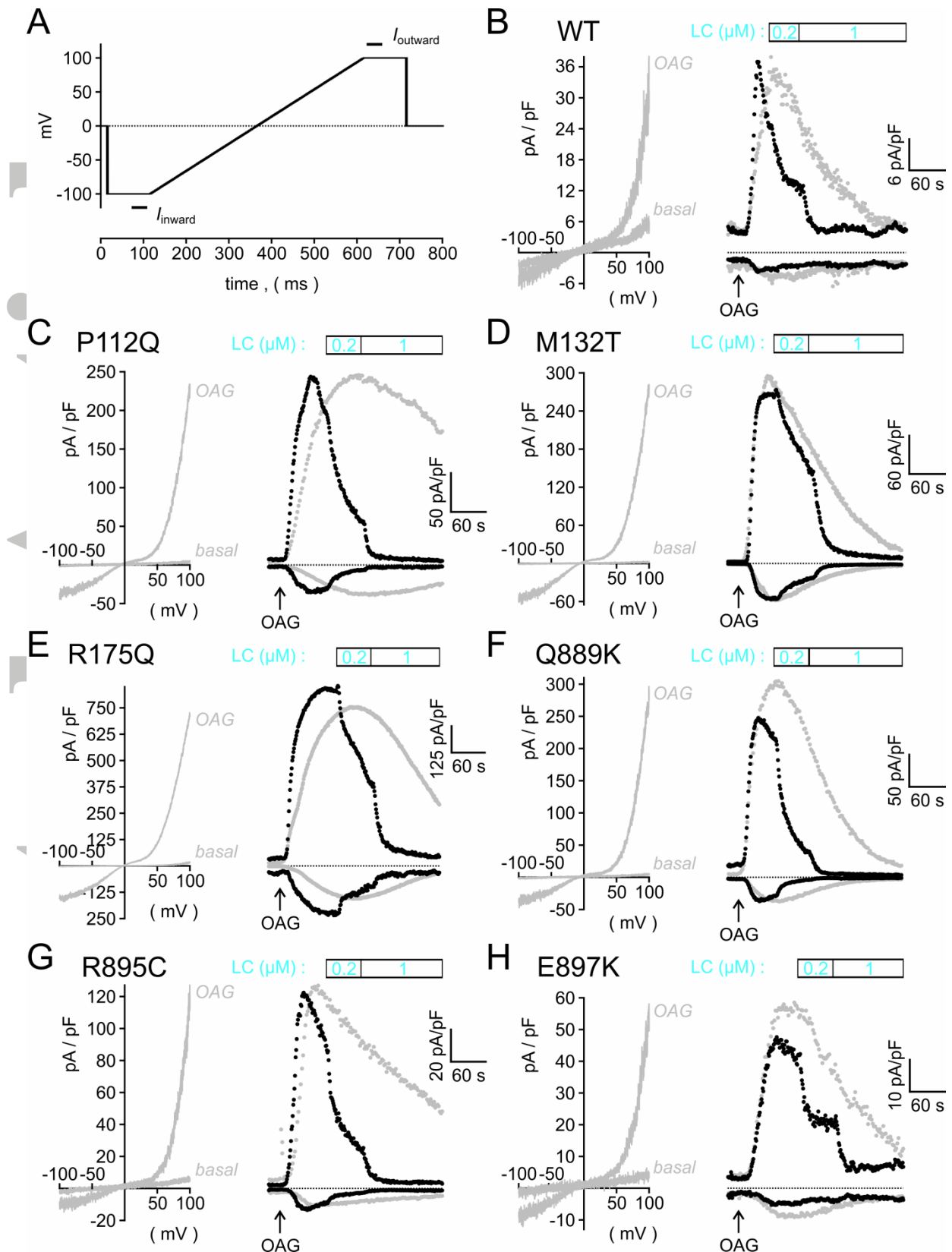


Figure 4: Inhibition of ionic currents through FSGS-related TRPC6 mutants by LC

Electrophysiological patch-clamp recordings were obtained in the voltage-clamped whole-cell mode. (A) Voltage protocol applied in the experiments. Horizontal bars indicate the time

Accepted Article

spans used for averaging inward and outward currents at -100 mV and +100 mV, respectively. The sweep frequency was 1 s^{-1} , and the inter-sweep holding potential was 0 mV. (B-H) Representative examples of whole cell currents elicited in HEK293 cells that were transiently transfected with expression plasmids encoding the indicated point-mutated TRPC6 channel variants. Whole cell currents were recorded during stimulation with 50 μM OAG either without subsequent application of LC (grey symbols and lines) or during sequential addition of 0.2 μM and 1 μM LC (black symbols and lines). Left panels: examples of currents measured during the application of voltage ramps before (basal) and shortly after the addition of OAG. Right panels: time course of inward currents at $V_h = -100 \text{ mV}$ (lower traces) and outward currents at $V_h = +100 \text{ mV}$ (upper traces). Note the different scaling of current densities between cells expressing wild-type (WT) or point-mutated TRPC6 constructs.

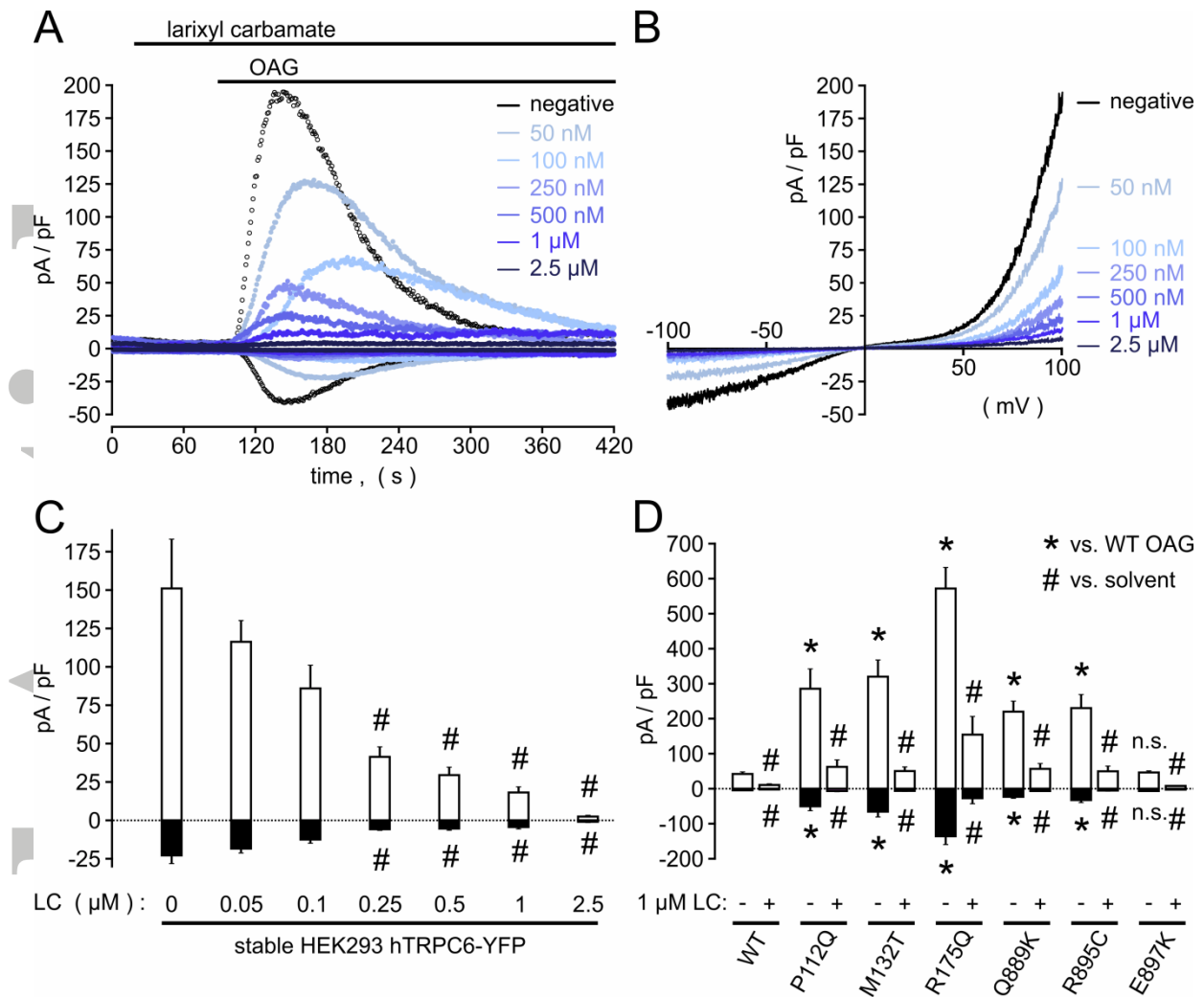


Figure 5: Pretreatment with LC concentration-dependently suppresses ionic currents through TRPC6, and potently inhibits FSGS-related TRPC6 mutants

Electrophysiological recordings of whole cell currents were performed as in Figure 4, but with the indicated concentrations of LC preincubated 60 s before challenging cells with 50 μM OAG. (A) Representative recordings of inward (lower traces) and outward current densities (upper traces) elicited in stably transfected HEK_{hTRPC6-YFP} cells by 50 μM OAG in the absence (negative) or in the presence of the indicated concentrations of LC. (B) Current density-voltage relationship of OAG-induced currents recorded during the respective outward current peaks in (A). Traces obtained in the presence of the indicated concentrations of LC are superimposed. (C) Statistical analysis (means and S.E.) of several experiments performed as shown in (A). OAG-induced peak outward (open bars) and inward (black bars) current densities were determined in 6-13 cells preincubated for 1 min with various concentrations of LC. #: significant ($p < 0.05$) lower current amplitudes compared to recordings in the absence of LC. (D) Experiments and statistical analysis as in (A) and (C), but with transiently transfected HEK293 cells expressing either wild-type (WT) or point-

Accepted Article

mutated TRPC6 constructs. Mean outward (open bars) and inward (black bars) current densities and S.E. were obtained without (-) or with (+) 1 μ M LC, preincubated for 60 s prior to current induction with 50 μ M OAG. Significant ($p < 0.05$) differences of OAG-induced current densities in point-mutated TRPC6 versus wild-type TRPC6 in the absence of LC (*) or significant inhibition of outward and inward current densities by 1 μ M LC (#) are indicated.

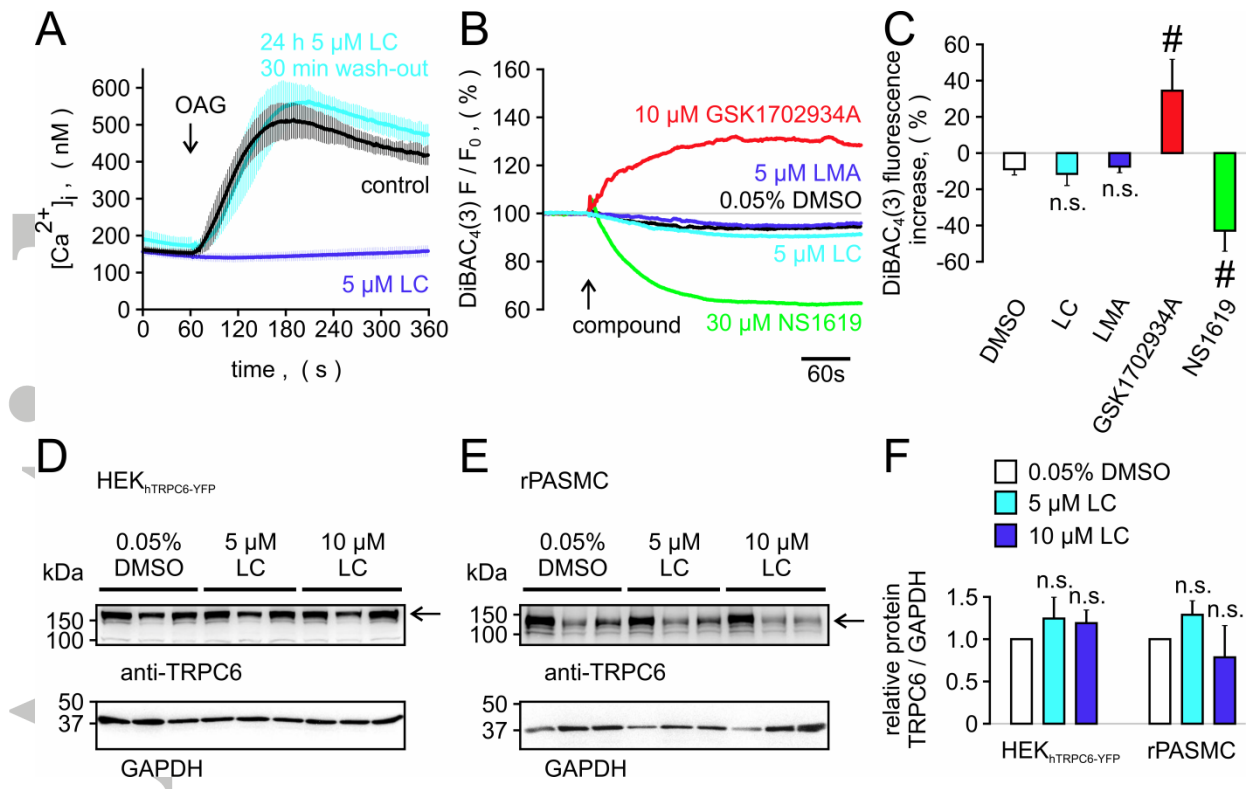


Figure 6: Effect of larixyl carbamate on basal TRPC6 expression and on membrane potential.

HEK293 cells stably transfected with human TRPC6 (A) or rat PASC (B) were incubated with 5 μ M LC, 10 μ M LC or with solvent for 24 hours. TRPC6 and GAPDH were assayed in the respective cell lysates by Western blot analysis. (C) Means and SD of 6-9 independent treatments for each condition. (D) To assess the effect of LC on TRPC6 surface availability, rat PASC were exposed to 5 μ M LC for 24 hours. Then, the TRPC6 inhibitor was washed out, PASC were loaded with fura-2/AM and subjected to single-cell $[Ca^{2+}]_i$ imaging. During continuous recording of $[Ca^{2+}]_i$, TRPC6 was activated by 100 μ M OAG. Control recordings were performed with untreated PASC (black trace), or with PASC, which were acutely incubated with 5 μ M LC before starting measurements (dark blue trace). Traces represent means and SD of 5-7 experiments. (E) Time course of DiBAC₄(3) fluorescence in rat PASC normalized to initial fluorescence (F₀) during exposure to 5 μ M LC (light blue), 5 μ M LMA (dark blue), 30 μ M NS1619, 10 μ M GSK1702934A (red) or solvent (black). Traces represent means of 5-8 individual recordings, each comprising the averaged signal from 60-120 cells. (F) Statistical analysis of peak changes in DiBAC₄(3) fluorescence measured as in (E) after compound addition (means and SD). #: significant differences (p < 0.05) from solvent controls.

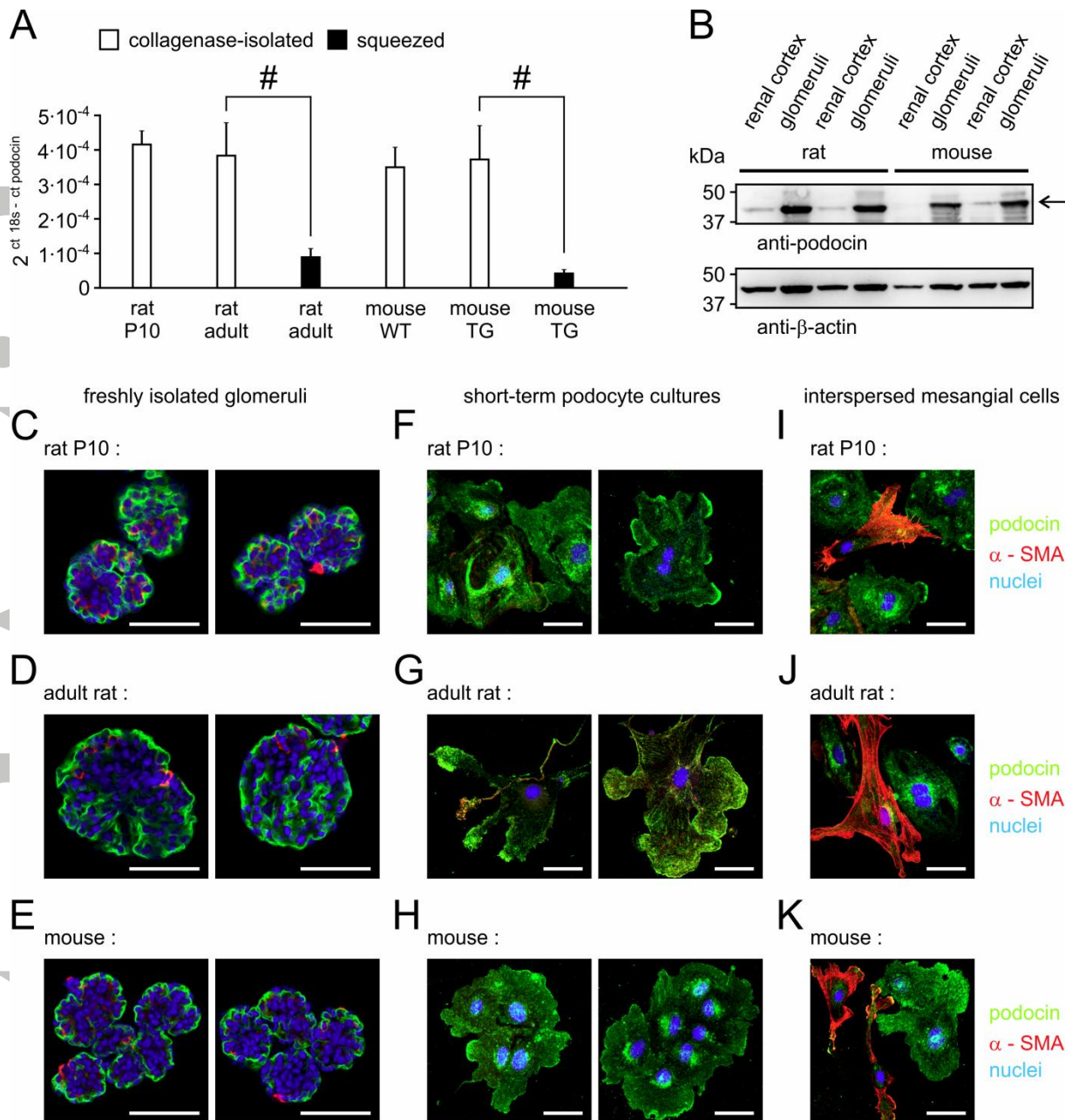
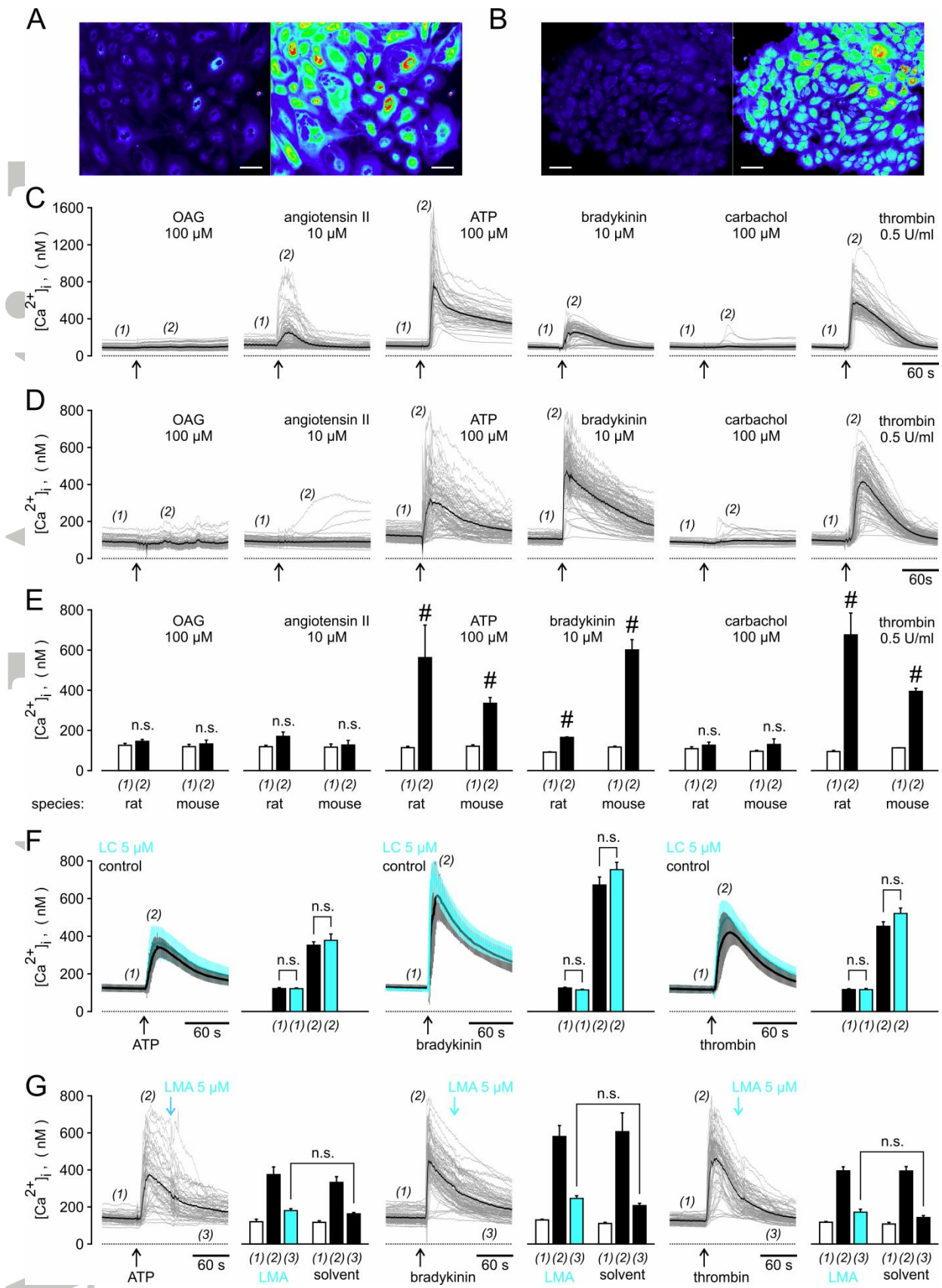


Figure 7: Isolation methods and culturing of glomeruli to obtain podocin-expressing podocytes.

Glomeruli from 10-days old rats, adult rats or from mice were isolated from the renal cortex by fractional sieving. Purity and podocyte enrichment strongly depend on the dissociation method. (A) Relative levels of podocin transcripts respective to 18s RNA yield were determined by quantitative real-time RT-PCR after isolation by mechanical squeezing through the first sieve (filled black bars) or by sieving after collagenase treatment and

Accepted Article

repetitive aspiration and suspension with a pipette (open bar). Shown are means and S.E. of 5-7 preparations for each species. (B) Exemplary Western blots depict the enrichment of the podocyte-specific marker podocin and of β -actin in glomeruli from rat and mouse kidneys obtained by the collagenase isolation method compared to the starting material (renal cortex). (C,F,I) Immunofluorescence staining and confocal imaging of podocin (green), α -SMA (red) and nuclei (blue) in freshly isolated decapsulated (collagenase treatment) rat and mouse glomeruli. Same stainings, but applied to short-term podocyte cultures, displaying pure podocyte groups (D,G,J) or cell groups with interspersed mesangial cells (E,H,K). White bars: 50 μ m.



Podocyte cultures were obtained from rats (A,C) or from transgenic B6.Cg-Tg(NPHS2-Trpc6) F419Walz/J mice (B,D,F,G), loaded with fura-2/AM, and subjected to single cell $[Ca^{2+}]_i$ analysis. (A) Imaging of basal (left panel) and ATP (100 μ M)-stimulated $[Ca^{2+}]_i$ in rat podocytes. The rainbow pseudocolor scale ranges from 0-800 nM. (B) Experiment as in (A), but with mouse podocytes challenged with 10 μ M bradykinin. (C) Representative recordings of $[Ca^{2+}]_i$ in single rat podocytes (grey traces) and averaged signals (black traces) during application of 100 μ M OAG or of the indicated agonists or activators of GPCR signalling. (D) Similar experiments as in (C), but using podocyte cultures obtained from TRPC6-overexpressing transgenic mice. (E) Statistical analysis of 4-10 experiments performed as in (C) and (D). Means and S.E. of basal $[Ca^{2+}]_i$ (open bars) and of the $[Ca^{2+}]_i$ after addition of the indicated modulators (black bars) are shown. Changes remained not significant (n.s.), or reached statistical significance at $p < 0.05$ (#). (F) $[Ca^{2+}]_i$ in primary podocytes from B6.Cg-Tg(NPHS2-Trpc6) F419Walz/J mice with (blue traces) or without (black traces) 5 μ M LC pre-incubation, and during stimulation with 100 μ M ATP, 10 μ M bradykinin or 0.5 units/ml thrombin. Left panels: averaged time course of $[Ca^{2+}]_i$ and SD calculated from 6-15 individual measurements. Right panels: statistical analysis (means and S.E. of 5-6 experiments, each) of peak responses. (G) Experiments similar as in (F), but with 5 μ M LMA (left panels) or solvent acutely added 60 s after GPCR stimulation. The statistical analysis (right panels) of 4-6 independent experiments, each, reveals no significant effect of the TRPC6 inhibitor on $[Ca^{2+}]_i$ if given 60 s after GPCR activation. White bars in (A,B): 100- μ m scale.

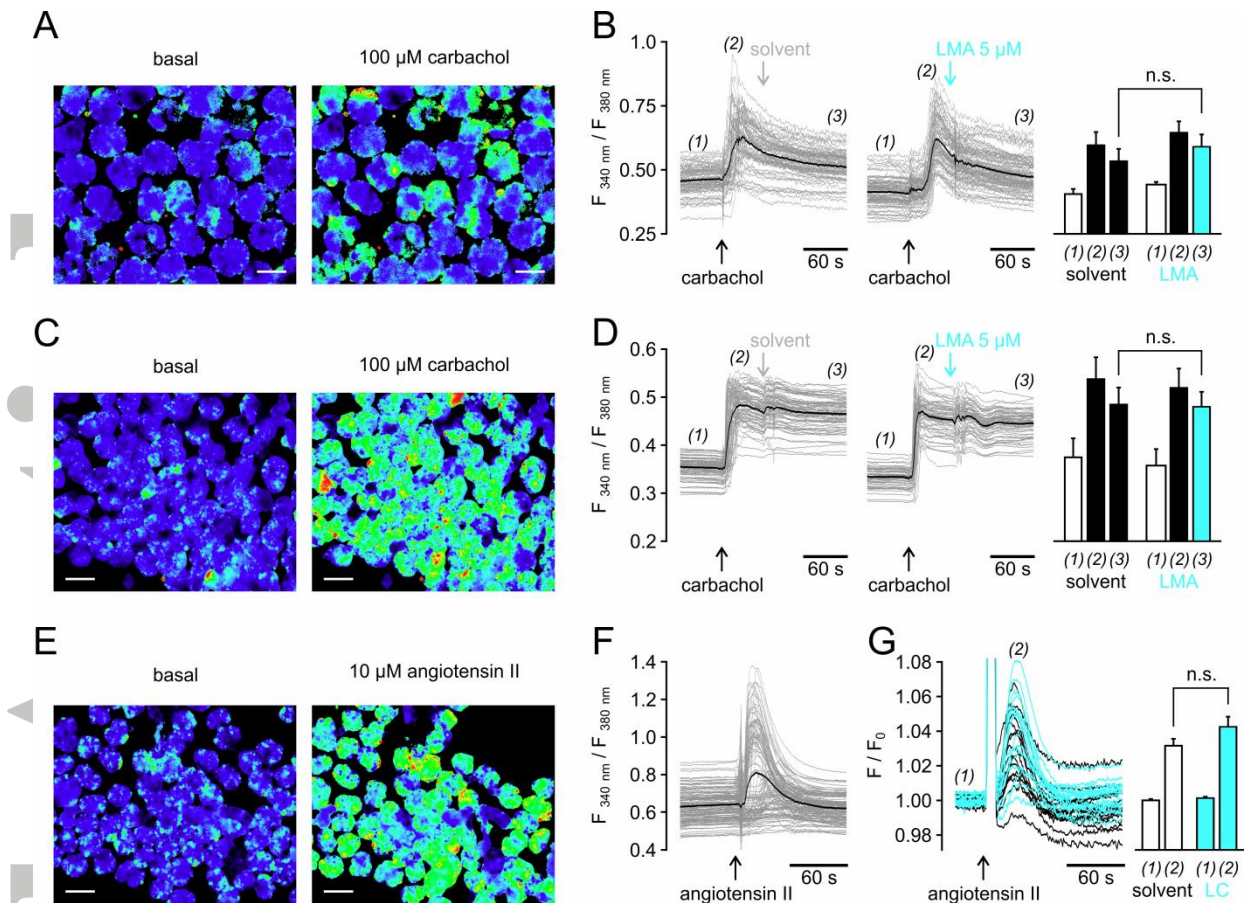


Figure 9: Ca^{2+} signals in acutely dissociated rat or mouse glomeruli are not significantly affected by LMA or LC

Glomeruli from 8-weeks old Wistar rats (A,B) or from 4-weeks old B6.Cg-Tg(NPHS2-Trpc6) F419Walz/J mice (C,D) were isolated by mechanical dissociation, collagenase treatment and fractional sieving. Glomeruli suspensions were loaded with fura-2/AM washed, and transferred to bath chambers for microfluorometry (A-F) or loaded with fluo-4/AM, washed and dispensed into microwell plates for imaging on a fluorescence plate imager (G). To elicit increases in $[\text{Ca}^{2+}]_i$ via stimulation of a phospholipase C-coupled GPCR, rat glomeruli were stimulated with 100 μM carbachol, followed by addition of 5 μM LMA or its solvent. (A) Representative background-corrected ratio images of $F_{340\text{ nm}}/F_{380\text{ nm}}$ before (basal) and 30 s after addition of 100 μM carbachol encoded with a rainbow pseudocolor scale ranging from 0.2 to 1.0. (B) Time course of $F_{340\text{ nm}} / F_{380\text{ nm}}$ in regions of interest defined within single glomeruli (grey traces), and averaged signals (black trace) during stimulation with carbachol without (solvent; left panel) or with subsequent addition of 5 μM LMA (middle panel). The right panel displays the statistical analysis of fluorescence ratios taken at the indicated time points in 5-6 independent experiments. (C-F) Similar experiments as in (A;B), but with glomeruli from TRPC6-overexpressing mice either stimulated with 100 μM carbachol (C;D)

or with 10 μM angiotensin II (E;F). Note that angiotensin II-induced $[\text{Ca}^{2+}]_i$ responses were seen in some but not all glomeruli. (E) To level out inhomogenous responses, experiments were therefore repeated in fluo-4-loaded glomeruli suspensions measured in a microwell plate imager with (blue traces) and without (black traces) preincubation with 5 μM LC (left panel). Statistical analysis of 16 measurements obtained in 3 independent experiments with glomeruli isolated from different animals. Signals with and without pretreatment with 5 μM LC did not reveal a significant LC-sensitive component of angiotensin II-induced $[\text{Ca}^{2+}]_i$ signals (right panel). White bars in (A,C,E): 100- μm scale.

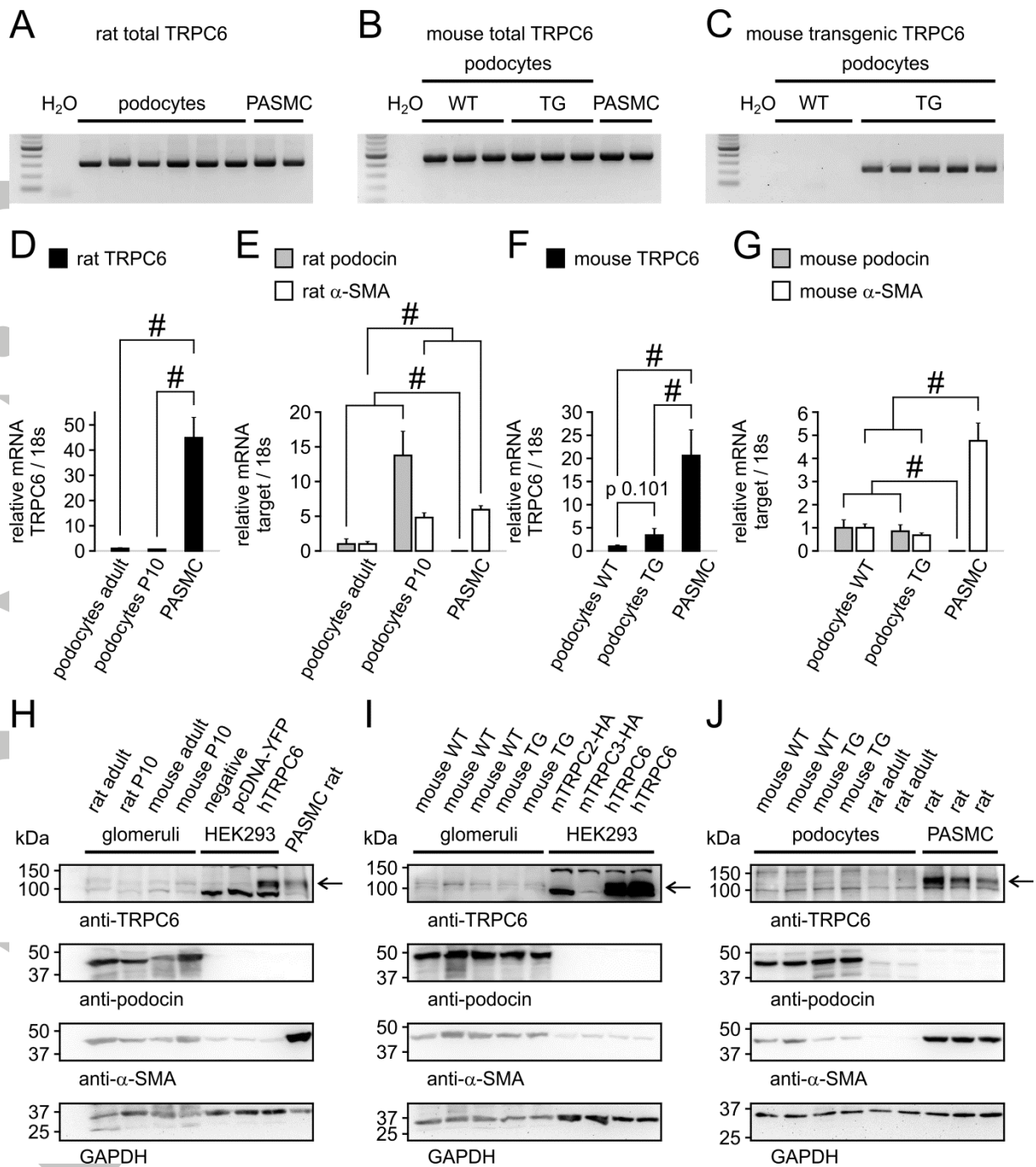


Figure 10: TRPC6 mRNA and protein abundance in murine podocytes and glomeruli compared to PASC

Quantitative RT-PCR was performed on RNA isolated from rat (A,D,E) and mouse (B,C,F,G) podocytes or PASC to detect total TRPC6, the TRPC6 transgene, podocin and α -SMA transcripts. Panels (A-C) depict PCR products obtained from podocyte and PASC cultures of different animals, and a water control with no RNA added to the RT-PCR (H₂O). Total (B) and transgenic (C) mouse TRPC6 expression was detected in wild-type (WT) and in transgenic B6.Cg-Tg(NPHS2-Trpc6) F419Walz/J (TG) mice. (D-G) Quantitative PCR results

from n = 6-11 experiments were normalised to 18s rRNA, and to the relative expression of the investigated mRNA in podocytes from adult wild-type animals. #: statistically significant ($p < 0.05$) differences between the indicated pairings. (H-J) Western blot analysis of TRPC6, podocin, α -SMA and GAPDH expression in acutely dissociated glomeruli, primary podocyte or PASMC cultures, and in untransfected or in HEK293 cells that were transiently transfected with expression plasmids encoding the indicated TRP channels or enhanced yellow fluorescent protein (YFP). If several lanes were loaded with the same condition, single lanes contain proteins obtained from a different animal. Shown are representative blots of 7 experiments with similar results.

Accepted Article

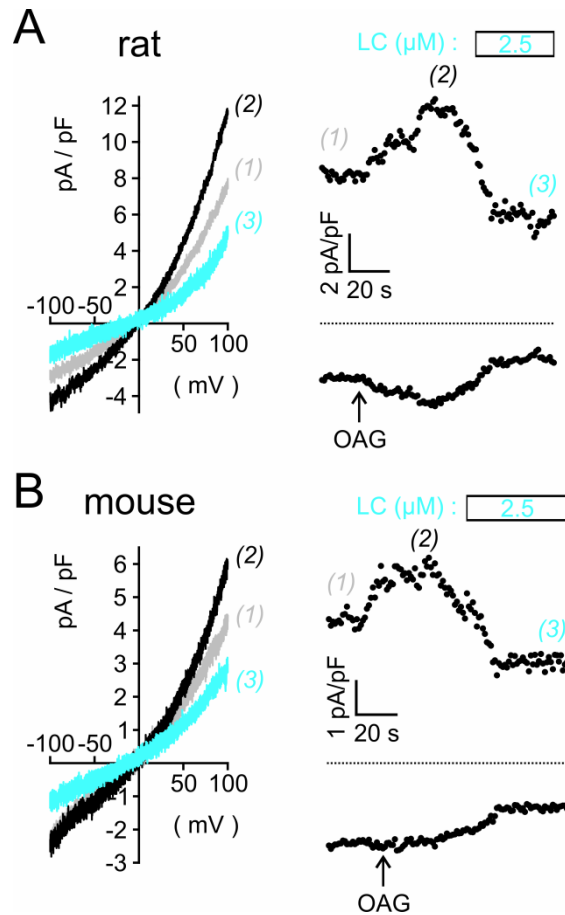


Figure 11: TRPC6-like ionic currents in primary rat and mouse podocytes are inhibited by LC

Whole cell currents were recorded in primary podocytes obtained from a Wistar rat (A) or from a Tg(NPHS2-Trpc6) F419Walz/J mouse, applying the voltage-ramp protocol described in Figure 5. Left panels: current density-voltage relationships before (grey line) and after sequential addition of 50 μM OAG (black line) and 2.5 μM LC (blue line) to the bath solution. Shown are raw data without leak subtraction. Right panels: time-course of inward currents at -100 mV (lower trace) and outward current densities at 100 mV over the whole experiment. Dotted lines: zero current level. Arrows and boxes indicate the time point of OAG and LC application, respectively.

Table 1: Basal and OAG-stimulated peak $[Ca^{2+}]_i$ in HEK cells expressing wild-type (WT) or FSGS-related point mutated forms of TRPC6. $[Ca^{2+}]_i$ was measured by single cell microfluorometry in fura-2-loaded HEK293 cells. Basal $[Ca^{2+}]_i$ before and OAG (50 μ M)-induced par $[Ca^{2+}]_i$ after TRPC6 activation were averaged over 150-200 cells, and n = 6 experiments were performed to calculate means \pm S.E.M..

| | basal $[Ca^{2+}]_i$ (nM) | compared to WT | OAG-induced peak $[Ca^{2+}]_i$ (nM) | compared to WT |
|-------|-----------------------------|----------------|--|-------------------|
| WT | 57.1 \pm 4.3 | | 124.3 \pm 17.5 | |
| P112Q | 78.9 \pm 5.6 | p = 0.011 | 248.8 \pm 29.0 | p = 0.004 |
| M132T | 153.8 \pm 19.2 | p < 0.001 | 286.0 \pm 25.8 | p < 0.001 |
| R175Q | 69.8 \pm 4.2 | p = 0.061 | 354.3 \pm 45.2 | p < 0.001 |
| Q889K | 71.2 \pm 1.4 | p = 0.011 | 280.0 \pm 46.1 | p = 0.010 |
| R895C | 78.4 \pm 6.6 | p = 0.022 | 168.3 \pm 20.8 | p = 0.137 |
| E897K | 63.8 \pm 3.2 | p = 0.238 | 184.5 \pm 52.6 | p = 0.302 |

Table 2: FRET efficiencies between coexpressed CFP-fused wild-type TRPC6 and point-mutated TRPC6 constructs. The molar ratio was quantified by comparing CFP and YFP fluorescence intensities (CFP measured after photobleaching of YFP) to those observed in an intramolecularly fused CFP-YFP construct. The FRET efficiency is calculated from the donor (TRPC6-CFP) fluorescence increase during selective photobleaching of the acceptor fluorochrome (YFP). Data represent means and S.E.M. of 17-27 photobleaching experiments.

| YFP | CFP | YFP / CFP molar ratio | FRET efficiency (%) | compared to WT |
|-------|-----|-----------------------|---------------------|----------------|
| WT | WT | 1.21 ± 0.1 | 18.0 ± 0.9 | |
| P112Q | WT | 1.23 ± 0.1 | 18.6 ± 1.0 | p = 0.670 |
| M132T | WT | 1.17 ± 0.1 | 19.0 ± 1.4 | p = 0.544 |
| R175Q | WT | 1.17 ± 0.1 | 15.9 ± 0.6 | p = 0.059 |
| Q889K | WT | 1.13 ± 0.1 | 18.5 ± 1.0 | p = 0.745 |
| R895C | WT | 1.17 ± 0.1 | 15.7 ± 0.7 | p = 0.051 |
| E897K | WT | 1.17 ± 0.1 | 19.7 ± 1.1 | p = 0.250 |